Copyright Warning & Restrictions

The copyright law of the United States (Title 17, United States Code) governs the making of photocopies or other reproductions of copyrighted material.

Under certain conditions specified in the law, libraries and archives are authorized to furnish a photocopy or other reproduction. One of these specified conditions is that the photocopy or reproduction is not to be "used for any purpose other than private study, scholarship, or research." If a, user makes a request for, or later uses, a photocopy or reproduction for purposes in excess of "fair use" that user may be liable for copyright infringement,

This institution reserves the right to refuse to accept a copying order if, in its judgment, fulfillment of the order would involve violation of copyright law.

Please Note: The author retains the copyright while the New Jersey Institute of Technology reserves the right to distribute this thesis or dissertation

Printing note: If you do not wish to print this page, then select "Pages from: first page # to: last page #" on the print dialog screen

ABSTRACT

NANOPOROUS SiO_2/VYCOR MEMBRANES FOR AIR SEPARATION

by
Mihir Tungare

Porous Vycor tubes with 40Å initial pore diameter were modified using low pressure chemical vapor deposition (LPCVD) of silicon dioxide (SiO_2). Diethylsilane (DES) in conjunction with nitrous oxide (N_2O) was used as a precursor to synthesize these SiO_2 films. The aim of this study was to obtain a considerable selectivity between species of comparable size and hence N_2O was used. The use of N_2O was believed to make the process self-limiting. DES was allowed to flow through the tube and N_2O on the outside in the chamber at 550°C in a counter-flow mechanism. This deposition geometry provided an optimum pore narrowing rate and eliminated the possibility of film cracking. The pore size of the Vycor tube was reduced with successive depositions and the stage at which maximum selectivity between oxygen and nitrogen was obtained was recorded. The value of selectivity was confirmed using mass spectroscopy and reproducing the results using another Vycor tube. The temperature dependence on selectivity was also studied. Characterization of the Vycor membranes was carried out to observe the SiO_2 coating. Calculation of permeability was done using ASTM standards.

NANOPOROUS SiO_2/VYCOR MEMBRANES FOR AIR SEPARATION

by
Mihir Tungare

A Thesis
Submitted to the Faculty of
New Jersey Institute of Technology
in Partial Fulfillment of the Requirements for the Degree of
Master of Science in Materials Science and Engineering

Interdisciplinary Program in Materials Science and Engineering

August 2000

APPROVAL PAGE

NANOPOROUS SiO_2/VYCOR MEMBRANES FOR AIR SEPARATION

Mihir Tungare

Dr. Roland A. Levy, Thesis Advisor — Date
Distinguished Professor of Physics, NJIT

Dr. James M. Grow, Committee Member — Date
Professor of Chemical Engineering, Chemistry, and
Environmental Science, NJIT

Dr. Trevor A. Tyson, Committee Member — Date
Assistant Professor of Physics, NJIT

BIOGRAPHICAL SKETCH

Author: Mihir Tungare

Degree: Master of Science in Materials Science and Engineering

Date: August 2000

Undergraduate and Graduate Education:

- Master of Science in Materials Science and Engineering,
  New Jersey Institute of Technology, Newark, NJ, 2000

- Bachelor of Engineering in Metallurgy,
  Govt. College of Engineering, Pune, India, 1999

Major: Materials Science and Engineering

To my parents, Mama and Baba, and my brother, Subeer

ACKNOWLEDGMENT

I would like to express my sincerest gratitude to Dr. Roland A. Levy, for his advice, guidance, and encouragement. Those hard pats on my back surely boosted my confidence. His knowledge and experience helped me deal with various problems in the CVD research lab. I am thankful to Dr. James M. Grow and Dr. Trevor A. Tyson for reviewing my thesis and providing me with some enlightening discussions. Special thanks to Dr. Peter C. Foller and PPG industries for discussing their concerns and having faith in me. Their valuable comments were of great help. I am grateful to Dr. Date for encouraging me in pursuing a higher degree and for all those cheers and good wishes.

I would like to express my appreciation to my CVD lab-mates Narahari Ramanuja and Dian Hong Luo for their support, helpful discussions and companionship. The jokes and humor filled conversations helped ease the burden of work and academics. I thank Narahari, my lab partner, in guiding me during the initial stages of my research and wish him luck as he steps into his future at Intel. Thanks to Kenneth J. O'Brien for his technical assistance with equipment and his entertaining conversations.

I am also grateful to my friends Anto, Bhavin, Lim, Yew Fong, Kunal, Animesh, Tushar, Nimish, Chetan, Ravinder, Pawan, and many others who were always there when I needed them.

I thank Mama, Baba, Subeer, Aba, Nanchi, and Shonu for their love and that long-distance support and inspiration. I am grateful to Sandhya aunty and Ashok uncle for all the help they provided.

...and to all whom I failed to mention who were instrumental for the completion of this endeavor, I express my sincerest thanks.

TABLE OF CONTENTS

Chapter	Page
1 INTRODUCTION	1
1.1 Air Separation Sparks Ceramic Membrane Technology	1
1.2 Development in Ceramic Membranes	5
1.3 Ceramic Membrane Materials and Applications	6
1.4 SiO_2 as a Membrane Layer	8
1.5 Use of DES as a Precursor Gas	9
2 SYNTHESIS OF CERAMIC MEMBRANES	12
2.1 Sol-Gel Technique	13
2.2 Slip Casting	14
2.3 Acid Leaching	15
2.4 Dense Membranes	16
2.5 Track Etch Method	17
2.6 Pyrolysis	17
2.7 Thin Film Deposition Methods	18
2.7.1 Physical Vapor Deposition	19
2.7.2 Chemical Vapor Deposition	22
2.7.2.1 Overview of the Chemical Vapor Deposition Process	22
2.7.2.2 CVD Reactor Systems	23
2.7.2.3 Nucleation and Growth	25
2.7.2.4 Chemical Reactions and Kinetics	26
2.7.2.5 Transport Phenomena	26
3 MEMBRANE CHARACTERIZATION AND GAS SEPARATION MECHANISMS	28
3.1 Pore Characterization	28

TABLE OF CONTENTS
(Continued)

Chapter	Page
3.1.1 Mercury Porosimetry	28
3.1.2 Nitrogen Adsorption/Desorption	29
3.1.3 Nuclear Magnetic Resonance	30
3.1.4 Permporometry	30
3.2 Characterization of the Structural Integrity of the Membrane	31
3.3 Gas Separation Mechanisms and Transport Phenomena	33
3.3.1 Gas Separation by Knudsen Diffusion	33
3.3.2 Gas Separation by Surface Diffusion	35
3.3.3 Gas Separation by Capillary Condensation	37
3.3.4 Gas Separation by Molecular Sieving	37
3.4 Entropic and Energetic Selectivity in Air Separation	39
4 EXPERIMENTAL PROCEDURE	42
4.1 Modified LPCVD Reactor	42
4.2 SiO_2/Vycor Membrane Fabrication	44
4.2.1 Predeposition Procedure	44
4.2.2 SiO_2 Deposition	45
4.3 Permeability and Selectivity Measurements	46
5 RESULTS AND DISCUSSION	47
5.1 Virgin Vycor Tube Measurements	47
5.2 Deposition of SiO_2 at 550°C	47
5.2.1 Membrane I	49
5.2.2 Membrane II	52
5.2.2.1 Characterization of Membrane II	56

TABLE OF CONTENTS
(Continued)

Chapter	Page
5.3 Effect of Temperature on Permeability	59
5.4 Calculation of Permeability	62
6 CONCLUSIONS	65
REFERENCES	67

LIST OF TABLES

Table	Page
1.1 Commercial ceramic membranes.....	4
1.2 Properties of Silica.....	10
1.3 Properties of DES.....	11
2.1 Evaporation vs. Sputtering.....	21
5.1 Viscosity of Oxygen as a Function of Temperature.....	60

LIST OF FIGURES

Figure		Page
1.1	Part of ceramic membranes in market	3
2.1	Schematic showing the transport and reaction processes underlying CVD	23
2.2	LPCVD Reactor	24
3.1	Schematic of bubble point test apparatus	32
3.2	Potential energy (E_p) along the permeation path of two molecules of different sizes, representing hydrogen and methane	38
4.1	LPCVD reactor for the synthesis of SiO_2 films on Vycor tubes	42
5.1	Plot of Permeability (across Membrane I) as a function of 1/Square root of Molecular Weight	48
5.2	Plot of Permeability as a function of 1/Square root of Molecular weight	49
5.3	Permeability as a function of Deposition time for Membrane I	50
5.4	Selectivity of Membrane I as a function of Deposition time	51
5.5	Linear dependence of dP/dt on Pressure difference for determination of Permeability for Membrane I	51
5.6	Permeability as a function of Deposition time for Membrane II	52
5.7	Selectivity of Membrane II as a function of Deposition time	53
5.8	Linear dependence of dP/dt on Pressure difference for determination of Permeability for Membrane II	53
5.9	Outgassing species within the tube	54
5.10	Gas sample from the tube with oxygen in the chamber	55
5.11	Gas sample from the tube with nitrogen in the chamber	56
5.12	Exterior surface of Vycor tube at a Magnification of 26X	57
5.13	Exterior surface of Vycor tube at a Magnification of 54X	57

LIST OF FIGURES
(Continued)

Figure		Page
5.14	Interior surface of Vycor tube at a Magnification of 54X.....	58
5.15	Cross section of Vycor tube at a Magnification of 54X.....	58
5.16	Cross section of Vycor tube at a Magnification of 54X.....	59
5.17	Temperature dependence of Permeability.....	61

CHAPTER 1

INTRODUCTION

1.1 Air Separation Sparks Ceramic Membrane Technology

Gas separation is important in processes involving oxygen enrichment, inert gas generation, air dehumidification, pollution control as well as hydrogen, helium, and hydrocarbon recovery[1,2]. It is also a subject of growing interest in studies concerned with the reduction in emission of volatile organic compounds (VOCs)[3,4]. Although there are a number of methods to achieve gas separation, such as adsorption-desorption techniques, controlled pressure distillation and cryogenic separation; separation by membranes is more desirable because of the simplicity, high processing flexibility and energy efficiency of the membrane separation process[5]. It is in this realm of separation technology that ceramic membranes have gained considerable interest and the improvements in their synthesis have been at a tremendous pace.

In the past, polymeric membranes[6] were used for separation of mixtures in process industries. On a large scale, these polymeric membranes were utilized in the oxygen enrichment of air, hydrogen separation from carbon monoxide and other gases, removal of carbon dioxide from natural gas, and the reduction of organic vapor concentration in air. Other, smaller scale applications include the preservation of food such as apples and bananas during transport by blanketing with low-oxygen-content air, the generation of inert gases for safety purposes, and the dehydration of gases[7]. Polymeric membranes continue to be an active area of research, with current emphasis on

specialized applications such as ion separation in electrochemical processes, membrane based sensors for gas and ion detection, and membrane reactors. Probably the largest area of active research in polymer membranes is in the biomedical field and the use of membranes in dialysis of blood and urine, artificial lungs and skin, the controlled release of therapeutic drugs, and the affinity separation of biological molecules. The distinguishing feature for polymeric membranes is that they contain a fibrillate structure and great size (macromolecules) which in turn result in cohesive forces which extend to the macroscopic level[8]. Moreover, because of relative ease of processing, the pore sizes and their distribution can be tailored to obtain any desired properties. However, despite their many advantages, polymeric membranes still cannot meet the demands of high temperature applications. One of the main reasons for this is the fact that polymers, being organic compounds[9] with relatively weak bonds, are unstable at high temperatures and soften to such an extent that they collapse under their own weight. Hence ceramic membranes have attracted scientific interest for so long. They offer a higher mechanical strength, are very resistant to organic solvents and many can be used in a rather wide pH and temperature range[10].

Quoting Dr. Yufei Gao[11], an engineer in the Environmental Sciences Division of Battelle's Pacific Northwest National Laboratory (PNNL), "Ceramic membranes exhibit unique physical and chemical properties that are only partially shown or not shown at all by polymeric membranes. For example, they can be used at significantly higher temperatures, and have much better mechanical stability without the swelling and shrinkage problems typically associated with polymeric membranes. They usually can

withstand more harsh chemical environments, are not subjected to microbiological attack, and can be backflushed, steam sterilized, or autoclaved".

Air separation has sparked ceramic membrane technology as these membranes can be effectively used for generation of ultra-sterile, high purity (>99.9%) oxygen for medical therapy, removing trace oxygen (<1ppb) in process gases and for gas analysis and calibration. They are also being used for controlled oxygen environments in food preservation and shipping of perishables. This attracted interest is reflected in the enhanced part of ceramic membranes in the future membrane market:

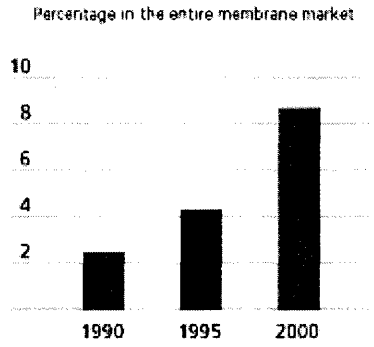

Figure 1.1 Part of ceramic membranes in market

To most users, ceramic membranes are a relatively new product. Ironically, their use extends over the past half of a century, starting with the development and mass production of membranes for the separation of uranium isotopes by the process of gaseous diffusion applied to UF_6. In the 80s, non-nuclear industrial applications were in place, mainly oriented towards microfiltration and ultrafiltration processes. They have evolved into important tools for beverage production, water purification, and the separation of dairy products[12]. The most recent research involves separations using a

variety of basic processes, including the coupling of catalytic reactions and membrane separations. Some years ago, the ceramic membranes employed for gas separations were typically based on the use of Knudsen diffusion as the primary mechanism of transport. However, currently available ceramic membrane technology allows one to utilize not only Knudsen diffusion but also surface activated transport as vehicles for bringing about molecular separations. Table 1.1 gives a list of some of the currently available inorganic ceramic membranes.

Table 1.1 Commercial ceramic membranes

Manufacturer	**Membrane material**	**Diameter of pores in the membrane**
US Filter	ZrO_2	20nm
US Filter	Al_2O_3	5nm
Alcan/Anotec	Al_2O_3	20nm
Gaston County Filtration Systems	ZrO_2	4nm
Rhone-Poulenc/SFEC	ZrO_2	4nm
TDK	ZrO_2	~10nm
Schott Glass	Glass	10nm
Fuji Filters	Glass	4nm

Currently available ceramic membranes possess pore diameters that are no less than 4nm in size. These are the membranes that are separating gases primarily by Knudsen and surface diffusions. But, the selectivity achieved is low. Through a uniform reduction of the pore size in the Vycor glass substrate down to a nanoscale level (~ 0.5nm), gas

separation can be dramatically enhanced due to the change in the gas transport mechanisms from the mesoporous to the nanoporous regime. In the mesoporous region where Knudsen diffusion dominates, selectivity is proportional to the inverse square root of the molecular weight ratio of the permeant gases[13-15]. In the nanoporous range, higher selectivity is primarily achieved as a result of molecular sieving effects[14,16,17] and other interesting mechanisms like entropic and energetic selectivity[18].

1.2 Development in Ceramic Membranes

Considerable effort has been exerted on the development of new types of inorganic membranes for gas separation and their application to a membrane reactor. Inorganic membranes reported can be classified into 2 groups from the viewpoint of raw material: ceramic membranes and metal membranes[19]. Various ceramic membranes, for example, not only porous ones with a narrow pore distribution, such as titania, zirconia, alumina, glass, molecular sieving carbon, silica and zeolite, but also dense ones without any pores or defects such as pervoskite, bismuth and solid-electrolyte, have been developed and commercialized. Inorganic membranes are more expensive than organic polymeric membranes, but ceramic membranes have the ability of providing extremely high filtration surface area and therefore great economy-of-scale, making them cost-effective[6]. Ceramic membranes are temperature and wear resistant. Ceramic membranes are in fact stable up to about 1000°C[20]. Ceramic membranes are processed by starting with assemblies of crystals and particles. As a result of the compact crystal structure and chemical bonding characteristic of the small and highly charged cations, ceramic membranes have very good structural integrity. This allows them to be used at the very

high pressures (~30atm) associated with high throughput. This obviously leads to more efficient energy use and economical savings. Porous membranes tend to have a well-defined, stable pore structure and are chemically inert, making them resistant to a wide variety of solvents, acids, alkalines, and detergents. These advantages encouraged researchers in the 1980's to investigate the gas separation properties and applications of ceramic membranes in membrane reactors. At present, the biggest challenge is to transfer the theoretical aspects of the technology to the applied aspects so valuable to industry. This study pertains to the production of nanoporous Vycor/SiO_2 membranes for the most important air separation application discussed earlier. The Vycor glass support provides mechanical strength to the membrane top layer to withstand the stress induced by the pressure difference applied over the entire membrane and simultaneously has a low resistance to the filtrate flow[21].

1.3 Ceramic Membrane Materials and Applications

Ceramic membranes can be deposited on a support or made as such in the form of a plate of active material[12]. Supported membranes are commonly used at high temperature. Usually, a ceramic film is deposited onto a substrate[22] that has a larger mean pore size. The substrate will typically be the load-bearing member of the membrane and therefore must maintain its mechanical integrity over a wide temperature and pressure range. Concurrently, the substrate also must be microcrack and defect free. It must be able to withstand the highly corrosive environment in which it is placed. The substrate has to have a large surface area to allow for high throughput with the mesopores providing all of the inherent permeability. Finally, these pores should be of a very narrow size

distribution. In this study, an additional property, the coefficient of thermal expansion comes into effect. This can be related to structural integrity at high temperatures, but for this application, the difference between the coefficients of thermal expansion for the support and the deposit should be as low as possible to reduce the possibility of microcrack formation in the membranes, the primary source of membrane failures.

The substrate used in our study was a porous Vycor glass tube manufactured by Corning Inc., and is commercially available as Vycor 7930. Vycor glass is made up of 96% SiO_2, the rest being B_2O_3. The special features of Vycor are as follows:

- Superior optical quality
- Tight dimensional control
- Thermal and chemical properties ideally suited to high temperatures
- Easy conversion from fused quartz
- Excellent thermal shock resistance

Typical ceramic materials include alumina, zirconia, titania, silica, carbon, and silicon carbide. These membranes can come in several configurations: hollow fibers, flat plates, honeycombs and hollow tubes.

These types of ceramic membranes find increasing use in the following applications:

- gas separation: involves mainly the removal of hydrogen from refinery stream, and carbon dioxide and hydrogen sulfide from natural gas.
- biotechnology/pharmaceutical: Removal of viruses from culture broth and purification of amino acids, vitamins, and organic acids.

- petrochemical: catalytic dehydrogenation[22] of large molecules at low temperatures and also used for coal gasification.
- environmental control: To get rid of precipitated radionuclides and metaloxides.
- concentration and homogenization of milk and eggs.
- metal refining: removal of impurities and undesirable metal oxides from superalloys.

Innovative applications are still being discovered such as an integrated membrane[24]. This composite membrane consists of a selective layer and a catalytic layer. The selective layer allows the migration of only the reactant and blocks the impurities. The reactant then comes in contact with the catalytic layer where it is converted into the product and is subsequently swept off by convective forces. The benefits of such a process are highly simplified processing, no byproducts, and faster kinetics. A prototype has been developed for use in hydrocarbon oxidation and hydrogenation processes.

1.4 SiO_2 as a Membrane Layer

Silicon dioxide proves to be the best choice as a membrane layer due to the matched coefficients of thermal expansion between the film and the substrate, which would minimize film cracking during thermal cycling[8]. Films of SiO_2 were deposited using diethylsilane (DES) and N_2O, diethylsilane being the source of silicon and Nitrous oxide the source of O_2. Silicon dioxide films produced from DES have been shown to exhibit better conformality, lower stress, and higher crack resistance than those produced from SiH_4[26-28]. Besides silane[29,30], other reported precursors used in the synthesis of CVD SiO_2 films for membrane applications include $SiCl_4$[31,32] and triisopropylsilane[33]. Oxygen was the most commonly used precursor in the CVD synthesis of SiO_2 films[28-30,33], until

the study started by Levy[34] et al where N_2O was first used. In that study, the use of N_2O as a precursor gas was believed to make the process self-limiting. When the pore diameter approaches the size of the N_2O molecule, no further reactions would be expected and film deposition would automatically stop. The selection of N_2O with a diameter less than that of a typical VOC but greater than that of N_2 would block the flow of the larger sized molecules while still permitting N_2 to flow through the membrane. Also, silicon dioxide has some very attractive inherent properties that make it a potential competitor as a membrane material. SiO_2 has low moisture absorption and low compressive stress. The principal physical properties of SiO_2 are given in Table 1.2.

1.5 Use of DES as a Precursor Gas

Extensive work has been done on the chemical vapor deposition of silicon dioxide thin films on various substrates including silicon, quartz, and glass[26-31]. A wide range of precursors have been used as a source for silicon to obtain these thin films including silane[29,30], silicon tetrachloride[31,32], triisopropylsilane[33], and diethylsilane[26-28]. DES is a colorless liquid with a boiling point of 56°C and a freezing point of -76°C. It has a high enough vapor pressure (207torr at 20°C) for easy delivery and control of the gas in the LPCVD reactor. In fact, DES can be sent into the reactor without the need of a carrier gas. Heating of the liquid source and the delivery line is not necessary either. Also attractive is the fact that DES is environmentally benign, satisfying any safety or environmental concerns. The properties of DES are given in Table 1.3.

Table 1.2 Properties of silica

Boiling Point (°C)	~2950
Melting Point (°C)	~1700
Molecular Weight	60.08
Refractive Index	1.46
Specific Heat (J/g°C)	1.0
Stress in Film on Si (dyne/cm^3)	2-4 x 10^9, compressive
Thermal Conductivity (W/cm°C)	0.014
DC Resistivity (Ω-cm), 25°C	10^{14}-10^{16}
Density (gm/cm^3)	2.27
Dielectric Constant	3.8-3.9
Dielectric Strength (V/cm)	5-10x10^6
Energy Gap (eV)	~8
Etch rate in Buffered HF (nm/min)	100
Linear Expansion Coefficient (cm/cm°C)	5x10^{-7}

Table 1.3 Properties of DES

Chemical Name	Diethyl silane (DES)
Chemical Formula	$SiH_2(C_2H_5)_2$
Molecular Weight (g/mol)	88.2
Specific Gravity (g/cm^3 @ 20°C)	0.6843
Freezing Point (°C @ 1 atm)	<-76
Boiling Point (°C)	56
Appearance	Colorless liquid
Vapor Pressure (torr @ 20°C)	207
Vapor Density (air = 1)	> 1

CHAPTER 2

SYNTHESIS OF CERAMIC MEMBRANES

Membranes can be defined as semipermeable barriers that prevent intimate contact between two phases. These could be gaseous, liquid, solid, or a combination of such phases. The usefulness of membranes is primarily influenced by the capability to selectively restrict the movement of certain molecules while allowing others to pass, known as the permselectivity property of that membrane. The ideal membrane for gas separations has two characteristics; it is selective and permeable[35]. Selective membranes produce a high purity gas and permeable membranes provide a large flux. Unfortunately these qualities are often inversely related: as selectivity increases, flux decreases and vice versa. Changes in membrane chemistry have not completely overcome this limitation.

An increase in total flux of 5 times or more could revolutionize the gas separation industry. To seek this increase, membrane chemistry and hence membrane selectivity is fixed and focus is on achieving faster flux via improvements in geometry. There are two current ways to improve membrane geometry:

- Making the membrane as thin as possible
- Increase membrane area/volume, thereby speeding separation

This brief description shows the importance of the various methods used to synthesize ceramic membranes. An overview of these methods is provided in the text that follows.

2.1 Sol-Gel Technique

The sol-gel process can be divided into two main routes, the colloidal suspension route and the polymeric gel route[36]. In both cases, an inorganic salt or a metal organic precursor is hydrolyzed while simultaneously a condensation or polymerization reaction occurs. It is important that the hydrolysis rate with respect to the polycondensation rate be controlled. In the colloidal route, a faster hydrolysis rate is obtained by reacting the precursor with excess water. A precipitate of hydrated oxide particles is formed which is peptized in a subsequent step to a stable colloidal suspension. The elementary particle size ranges, depending on the system and processing conditions, from 3-15nm and these particles form loosely bound aggregates with sizes ranging from 5-1000nm. By increasing the concentration of the suspension and/or by manipulation of the surface potential of the sol particles the colloidal suspension is transformed to a gel structure consisting of interlinked chains of particles or agglomerates.

The hydrolysis and polymerization rate of metal organic compounds can generally be better controlled compared to those of metal salts. The chemical reaction involves two steps:

1. The partial hydrolysis of the metal organic compound introduces the active functional OH groups, attached to metal atoms.
2. These then react with each other or with other reactants to form a polymeric solution that further polymerizes to form a viscous solution of organic-inorganic polymeric molecules.

In the polymeric gel route, the hydrolysis rate is kept low by adding successively small amounts of water. The final stage of this process is a strongly interlinked gel

network with a structure different from that obtained from the colloidal route. This is because the network formation takes place continuously within the liquid. It is not necessary to remove this liquid to obtain a gel as in the colloidal route[37,38].

The size of the particles in the sol strongly determine the size of the final pore and can be tailored by changing the pH of the medium, the molar ratios of metal organics, temperature, feed rate of the reactants, etc. The particles have to be uniformly[39] distributed in the medium to obviate any non-uniform deposit. Also, the particles have to behave individually rather than act together as an agglomerate. For this purpose stabilizing or deagglomerating agents such as aliphatic acids, or bases are added to control the pH of the sol, thus inducing surface charge on the particles.

Sol gel technique is extensively used for alumina, zirconia and titania membranes. One of the main limitations of this technique is that the pore size is strongly dependent on the particle size, which cannot be obtained accurately. The final pore sizes rarely cross below the 4nm diameter and hence are useful for ultrafiltration. Research in this field is directed mainly at obtaining finer particles with diameters of approximately 3nm.

2.2 Slip-Casting

A common method to slip-cast[40] ceramic membranes is to start with the colloidal suspension or the polymeric solution of the sol-gel process described in the previous section. This is known as the slip. A porous substrate is dipped in the slip and a dispersion medium, i.e. water or water-alcohol mixtures, is forced into the pores of the support by a pressure drop created by capillary action of the microporous support[41]. At the interface, the solid particles are retained and concentrated at the entrance of the pores

to form a gel layer as in the case of sol-gel processes. It is important that formation of the gel layer starts immediately and that the solid particles do not penetrate the pores of the substrate system. This means that the solid concentration in the slip must not be too low, the slip must be close to its gelling state, and the particle size must not be too small compared with the pore size of the substrate. Smaller and more uniform the primary particles and weaker the agglomerates in the sol, the smaller the pore size and the narrower its distribution in the membrane. Rate of deposition of the membrane can be increased by increasing the slip concentration or by decreasing the pore size of the substrate.

The final stage is the firing of the gelled sol along with the support. A thorough understanding of the phase changes and thermal/hydrodynamic stresses developed during firing is essential to hold the membrane to the support.

2.3 Acid Leaching

Turner and Winks[31] first performed acid leaching in 1926 on glasses containing boric oxide using hydrochloric acid. By thermally demixing a homogenous Na_2O-B_2O_3-SiO_2 glass phase into two phases, glass membranes with an isotropic spongy structure of interconnected pores can be prepared. The alkali-borosilicate glass separates into a phase that is almost pure silica and a phase that is rich in Na_2O and B_2O_3. As the temperature is lowered, a tendency to form Na-O-B bonds rather than Na-O-Si bonds is developed. Simultaneous separation proceeds into an insoluble phase (-Si-O-Si-) and a soluble phase (-Na-O-B-)[32]. The latter phase is then leached either by an acid, base, or just water, thereby creating a porous structure in the SiO_2 phase. The pore size and distribution can

be controlled by the concentration of the leachable phase and by carefully monitoring the time and temperature during the thermal decomposition.

Acid leaching is a complicated process and extreme care has to be taken to obtain defect free porous glass. A strain is set up, partly from purely physical causes, because of capillary forces developing in the pores due to the presence of acid. The strain can be induced either by *swelling* of the leached layer or by *shrinking*. Glass is then scrubbed with water and dried slowly to remove excess water.

When the thermal treatment occurs at temperatures less than 400°C, the rate of redistribution of soluble component is slow and nucleation of the second phase does not occur[42]. Acid leaching at this stage results in a microporous glass with a pore size of 0.5 to 2nm. However, when the homogenous amorphous phase is thermally treated above 400°C, irreversible nucleation in the second phase begins. If the two-phase material is leached, a mesoporous glass membrane is formed. This is Vycor glass.

Vycor glass has a pore diameter ranging from 2-4nm and a porosity of about 30%. Porous Vycor glass can absorb atmospheric moisture by as much as 25% of its own weight. These glasses are commercially available as Vycor No. 7930, which is the substrate used in this study.

2.4 Dense Membranes

Dense membranes are essentially composite structures[43]. They consist of thin plates of oxides such as stabilized zirconia or bismuth oxides. These membranes are permeable to ionic forms of hydrogen or oxygen and are usually studied in conjunction with reactions like (oxidative) dehydrogenation, partial oxidation, etc. in membrane reactors[41,44]. Their

main drawback is their low permeability. This can be improved by making very thin micrometer or nanometer layers by deposition in a pore system.

2.5 Track Etch Method

In this process, particles from a radioactive source are passed through a material that eventually leaves a track. These tracks are highly sensitive to etchants and are hence etched using concentrated HF. It is possible to control the pore size, geometry, and density by monitoring the amount of radiation reaching the substrate surface.

The most remarkable feature of this technique is its ability to form linear pores with constant diameters. However, it is possible for only 2-5% of the material surface to be occupied by pores to prevent overlap[16,41].

2.6 Pyrolysis

Membranes with extremely small pores (< 2.5nm diameter) can be made by pyrolysis of polymeric precursors or by certain modification methods. Molecular sieve carbon or silica membranes with pore diameters of 1nm have been made by controlled pyrolysis of certain thermoset polymers or silicone rubbers, respectively[45]. When these materials are subjected to controlled pyrolytic conditions, volatiles are emitted and the compound collapses into a stable porous structure. Koresh and Sofer[46] have demonstrated the possibility of preparing highly selective carbon microporous membranes using pyrolysis. Further, Rao and Sircar developed what they called selective surface flow (SSF) membranes from poly(vinylidine chloride)-acrylate terpolymer latex coated on

macroporous graphite disks[74,75]. There has been continued emphasis on synthesizing molecular sieve structures using this approach.

Molecular sieve dimensions can be obtained by modifying the pore system of an already formed membrane structure. Zeolitic membranes can be prepared by reaction of alumina membranes with silica and alkali followed by hydrothermal treatment[43]. Oxides can be precipitated or adsorbed from solutions or by gas phase deposition within the pores of an already existing structure to modify the chemical nature of the membrane or to decrease the effective pore size. To decrease the pore size, a high concentration of the precipitated material in the pore system is required. This is essentially the aim of this study. Here, chemical vapor deposition (CVD) is employed to effectively reduce the pore size of a mesoporous membrane by depositing oxide in the pores. The aspect of this technology is being discussed next.

2.7 Thin Film Deposition Methods

Thin film deposition techniques have traditionally been used in the microelectronics industry for microchip coating, wear and corrosion resistance, and thermal protection. Although it is not necessary to produce a porous structure in the microelectronics applications, it is feasible to produce a porous structure by carefully controlling process parameters. Thin-film deposition essentially is used to narrow existing large pores (mesoporous) down to a size that is favorable for separation (microporous or nanoporous). Hence, a porous substrate is required which is free of defects such as cracks or pinholes. Compounds or elements are deposited inside the pores thus narrowing

down the pore size. Deposition methods can be classified into two groups: Physical Vapor Deposition (PVD) and Chemical Vapor Deposition (CVD).

2.7.1 Physical Vapor Deposition

Physical vapor deposition (PVD) is mainly divided into two categories, evaporation and sputtering. The objective of these deposition techniques is to controllably transfer atoms from a source to a substrate where film formation and growth proceed atomistically, without the need of a chemical reaction.

In evaporation, atoms are removed from the source by thermal means, whereas in sputtering the atoms are dislodged from a solid target by the impact of gaseous ions. The advances in vacuum-pumping equipment and Joule heating sources spurred the emergence of PVD as a suitable industrial film deposition process. In general, the properties of the film obtained by PVD are governed by the following: evaporation rate of the atoms, vapor pressure of the target materials, deposition geometry, temperature, pressure, and thermal history of the substrate[47].

Traditionally, evaporation was the preferred PVD technique over sputtering. Higher deposition rates, better vacuum (thus cleaner environments for film formation and growth), and versatility in the fact that all classes of materials could apply this technique were some of the reasons for the dominance of evaporation. The microelectronics revolution required the use of alloys with strict stoichiometric limits that had to conformally cover and adhere well to substrate surfaces. This facilitated the need for the sputtering technique and so, as developments were made in radio frequency, bias, and magnetron variants, so were advances made in sputtering. These variants extended the

capabilities of sputtering, as did the availability of high purity targets and working gases. The decision to use either technique depends solely on the desired application and has even spurred the development of hybrid techniques[47]. A comparison of the two is given in Table 2.1.

Some factors that distinguish PVD from CVD (discussed next) are:

1. Reliance on solid or molten sources
2. Physical mechanisms (evaporation or collisional impact) by which source atoms enter the gas phase
3. Reduced pressure environment through which the gaseous species are transported
4. General absence of chemical reactions in the gas phase and at the substrate surface (reactive PVD processes are exceptions)

Table 2.1 Evaporation vs. Sputtering

Evaporation	Sputtering
A. Production of Vapor Species	
1. Thermal evaporation mechanism	1. Ion bombardment and collisional momentum transfer
2. Low kinetic energy of evaporant atoms (@ 1200 K , E = 0.1eV)	2. High kinetic energy of sputtered atoms (E = 2-30eV)
3. Evaporation rate ~ 1.3 x 10^{17} atoms/cm^2-sec	3. Sputter rate ~ 3 x 10^{16} atoms/cm^2-sec
4. Directional evaporation according to cosine law	4. Directional sputtering according to cosine law at high sputter rates
5. Fractionation of multi-component alloys, decomposition, and dissociation of compounds	5. Generally good maintenance of target stoichiometry, but some dissociation of compounds
6. Availability of high evaporation source purity	6. Sputter targets of all materials are available; purity varies with material
B. The Gas Phase	
1. Evaporant atoms travel in high or ultrahigh vacuum (~ 10^{-6}-10^{-10}torr) ambient	1. Sputtered atoms encounter high pressure discharge region (~ 100mtorr)
2. Thermal velocity of evaporant 10^5 cm/sec	2. Neutral atom velocity ~ 5 x 10^4 cm/sec
3. Mean-free path is larger than evaporant-substrate spacing; evaporant atoms undergo no collisions in vacuum	3. Mean-free path is less than target-substrate spacing; Sputtered atoms undergo many collisions in the discharge
C. The Condensed Film	
1. Condensing atoms have relatively low energy	1. Condensing atoms have high energy
2. Low gas incorporation	2. Some gas incorporation
3. Grain size generally larger than for sputtered film	3. Good adhesion to substrate
4. Few grain orientations (textured films)	4. Many grain orientations

2.7.2 Chemical Vapor Deposition

Chemical vapor deposition uses chemically reactive vapors to synthesize or deposit a film or coating. This directly falls under the heading of pyrolysis, as well as disproportionation, reduction, and oxidation. Like PVD, this technique is also a valuable tool for the microelectronics industry. A very large variety of materials can be formed by this method, including those for membrane synthesis[48]. Film properties to control during CVD include thickness, composition, purity, crystallinity, and surface/bulk morphology. Fundamental issues in CVD, which relate directly to film properties, include thermodynamics, kinetics, mass transfer, momentum transfer, heat transfer, reactor design, and process control.

2.7.2.1 Overview of the Chemical Vapor Deposition Process: The individual process steps in the CVD technique are outlined as follows[49]:

1. Mass transport in the bulk gas flow region from the reactor inlet to the deposition zone.
2. Gas phase reactions leading to the formation of film precursors and byproducts.
3. Mass transport of film precursors to the growth surface.
4. Adsorption of film precursors on the growth surface.
5. Surface diffusion of film precursors to growth sites.
6. Incorporation of film constituents into the growing film.
7. Desorption of byproducts of the surface reactions.
8. Mass transport of byproducts in the bulk gas flow region away from the deposition zone towards the reactor exit.

Schematically, this is seen in Figure 2.1.

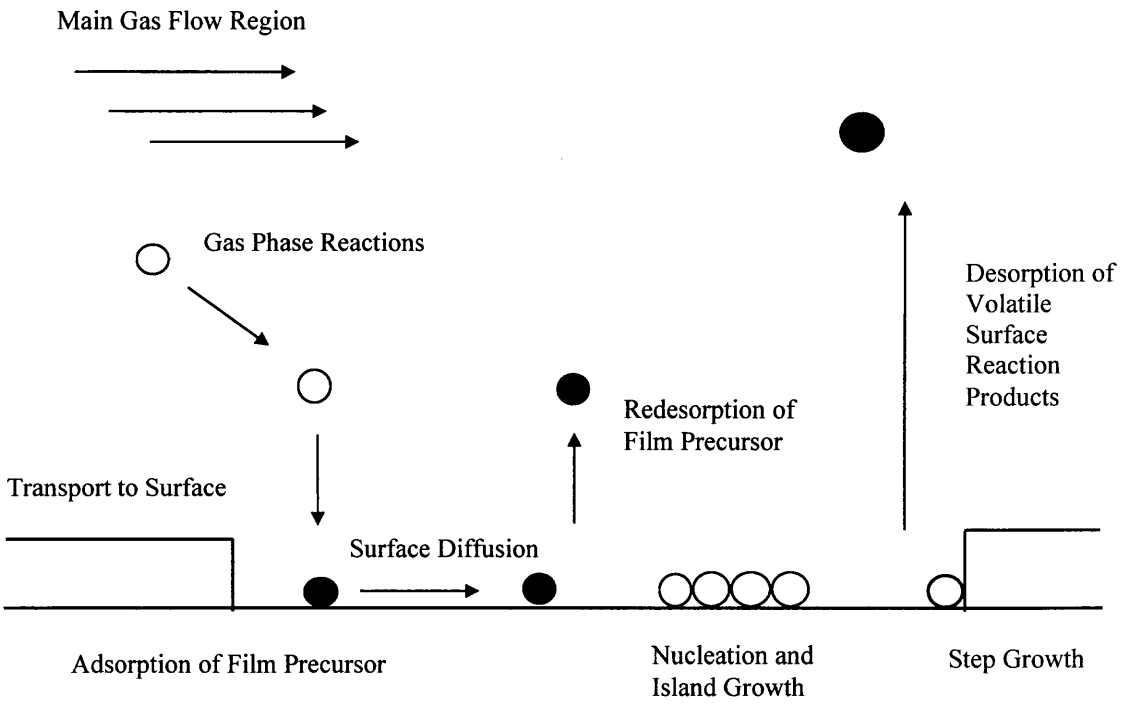

Figure 2.1 Schematic showing the transport and reaction processes underlying CVD

2.7.2.2 CVD Reactor Systems: CVD reactors are designed to obtain optimal film thickness, crystal structure, surface morphology, and interface composition. A CVD reactor system typically consists of a reagent handling arrangement for delivering the source compounds, a reactor unit, and an exhaust system. The reagent handling system mixes and meters the gas mixture to be used in the reactor. The design depends on the source compounds. Gaseous sources are fed from a high-pressure gas cylinder through a mass flow controller. Nitrous oxide is such a gaseous source used in the experiments that have been carried out. Liquid and solid sources are typically used along with a carrier gas in a bubbler. The source temperature, carrier gas flow rate, and the total pressure of the

source, determine the amount of reagent transported from the bubbler. In this study, a carrier gas is not needed because of the high vapor pressure of DES and the low-pressure nature of the deposition. The need for films with reproducible and controllable optical, electrical, and mechanical properties means that CVD reagents must be pure, must not produce byproducts that incorporate into the growing film or interact with gas handling and reactor construction materials.

There are a wide variety of CVD reactor geometries used to accommodate the many CVD applications. These include horizontal reactor, vertical reactor, barrel reactor, pancake reactor, and multiple-wafer-in-tube LPCVD reactor. Essentially, this study involves a multiple-wafer-in-tube LPCVD (low-pressure chemical vapor deposition) reactor modified to accommodate the membrane substrate (instead of wafers). LPCVD is the main production tool for polycrystalline silicon films, especially for the films used in the microelectronics industry[50-52]. A typical configuration for this reactor is shown below in Figure 2.2.

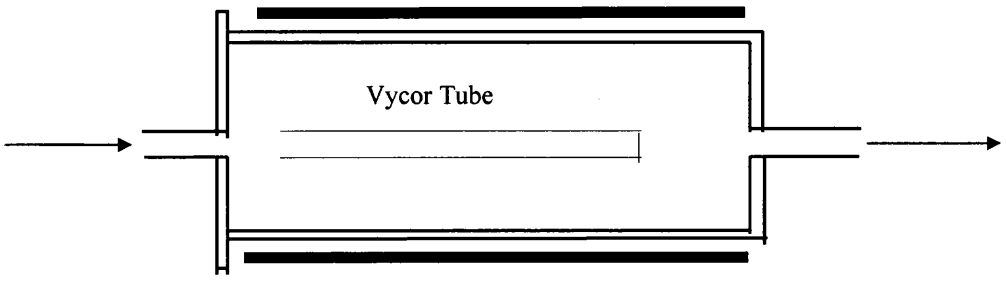

Figure 2.2 LPCVD Reactor

This reactor operates at a pressure of around 0.5torr and wall temperatures are approximately equal to those of the deposition surfaces. The main advantage of LPCVD is that it allows a large number of substrates to be coated simultaneously while maintaining film uniformity. This is a result of the large diffusion coefficient at low pressures, which makes the growth rate limited by the rate of surface reactions rather than the rate of mass transfer to the substrate.

Finally, the exhaust system treats the effluents so that hazardous byproducts are disposed off in a safe and environmentally sound manner. Mechanical pumps are typically added for the low-pressure operation. Dry and wet chemical scrubbers, as well as pyrolysis units, are used to clean up the reactor effluent.

2.7.2.3 Nucleation and Growth: The growth of a thin film by CVD is initiated by exposing a substrate to the film precursors in the reactor. The resulting growth and microstructure of the film is determined by surface diffusion and nucleation processes on the growth interface, which are influenced by the substrate temperature, reactor pressure, and gas-phase composition. An amorphous film is formed at low temperatures and high growth rates when the surface diffusion is slow relative to the arrival of film precursors. At high temperatures and low growth rates, the surface diffusion is fast relative to the incoming flux, allowing the adsorbed species to diffuse to step growth and to form epitaxial layers replicating the substrate lattice. Nucleation occurs at many different points on the surface at intermediate temperatures and growth rates. Adsorbed species then diffuse to the islands that grow and coalesce to form a polycrystalline film. The presence of impurities increases the nucleation density. CVD film growth modes may be

characterized in terms of three main growth models for thin films: Volmer-Weber growth (three-dimensional island growth), Franck-van der Merwe growth (two-dimensional layer by layer), and Stranski-Krastanov growth (layer plus island)[49].

2.7.2.4 Chemical Reactions and Kinetics: The versatility of the CVD technique is demonstrated through the multitude of films synthesized by various reaction schemes, including pyrolysis, reduction, oxidation, and disproportionation of the reactants. The underlying chemistry is typically a complex mixture of gas-phase and surface reactions. The fundamental reaction pathways and kinetics have been investigated for only a few well characterized, industrially important systems. These include silane chemistry (pertinent to this study and discussed in detail in the experimental procedure) and thus silicon deposition, free-radical reactions, and intramolecular reactions of organometallic compounds.

2.7.2.5 Transport Phenomena: Fluid flow, heat transfer, and mass transfer are all characterized under transport phenomena. Transport phenomena govern the access of film precursors to the substrate and also influence the degree of desirable and unwanted gas-phase reactions taking place before deposition. The complex reactor geometries and large thermal gradients of CVD reactors lead to a wide variety of flow structures impacting film thickness and composition uniformity, as well as impurity levels. Direct observation of flow is difficult because of a lack of a suitable visualization technique for many systems and because of practical constraints such as no optical access and possible

contamination of a production reactor. Therefore, experimental observations and approximately chosen computer models are employed on individual systems[53,54].

The complexity of transport phenomena can be observed by the variety of phenomena that have been observed even in single gas permeation. These involve[55]:

- For a particular gas the flux may increase with temperature at a given pressure and with a particular membrane, while a decrease is observed for membranes with different pore size or of another material.
- For some gases maxima in the flux as a function of temperature at a given pressure are observed, the temperature of this maximum being a function of pressure.
- The flux can increase linearly with feed pressure (permeance is constant), may increase strongly non-linear and eventually show saturation behavior depending on the temperature and on the particular gas-membrane combination.
- Usually at high temperature and for a given membrane the permeance decreases with increasing effective molecular diameter. However, for some conditions this trend is reversed.
- The flux (permeance) might be very sensitive for small changes in the permeance (low) pressure and the type of support.

CHAPTER 3

MEMBRANE CHARACTERIZATION AND GAS SEPARATION MECHANISMS

The separation efficiency, i.e. permselectivity and permeability, of ceramic membranes depends on microstructural features such as pore size and pore distribution, pore shape, and porosity. Also included in the microstructural characteristics of the membrane is its stability and structural integrity. Several techniques are available to characterize ceramic membranes. These are discussed along with the gas separation mechanisms involved in ceramic membranes. The pore size of the membrane directly affects the transport mechanism through the pores.

3.1 Pore Characterization

Pore size plays an important role in determining permeability and selectivity of a membrane. The structural stability of porous ceramic membranes under high pressures makes them amenable to conventional pore size analysis such as mercury porosimetry and nitrogen adsorption/desorption. Newer techniques which employ nuclear magnetic resonance technology and a method known as permporometry are also used[56,57].

3.1.1 Mercury Porosimetry

Pore diameter data in the range of 3.5-7500nm can be obtained using mercury porosimeters. The method is useful and very common in the characterization of membranes[58-60]. Mercury is non-wetting on most surfaces and has to be forced into the pore under pressure.

The relation between the pore size, r, and the applied pressure, P, is given by:

$$r = \frac{-2\gamma \cos\theta}{P} \tag{3.1}$$

Where, γ is the surface energy and θ is the contact angle between the pore walls and mercury. Typical mercury porosimetry data come in two forms, intrusion and extrusion. The intrusion data are more often used because the intrusion step precedes the extrusion step in the mercury porosimetry analysis and the complete extrusion of mercury out of the pores during the depressurization step of the analysis may take a very long time.

3.1.2 Nitrogen Adsorption/Desorption

This works well where mercury porosimetry does not, when the pore size is smaller than 3.5nm. In fact, it works well for pore sizes between 1.5 and 100nm. This method is based on the widely used BET theory[56]. The BET theory modifies Langmuir's work relating the volume of a gas adsorbed or desorbed to the relative pressure, p/p_o. Langmuir assumed a monolayer adsorption/desorption, while Brunauer, Emmett, and Teller account for multilayer adsorption/desorption. Typical data from this method are split into two portions: adsorption and desorption. The nitrogen desorption curve is usually used to describe the pore size distribution and corresponds better to the mercury intrusion curve.

3.1.3 Nuclear Magnetic Resonance

This method employs NMR spin-lattice relaxation measurements to characterize a wide range of pore sizes (<1 to >10000nm)[61]. Here, the moisture content of the membrane is controlled so that the fine pores in the membrane film are saturated with water, but only a small amount of adsorbed water is in the large pores of the structure. It is known that the spin-lattice relaxation decay of water in a pore is shorter than that for water in the bulk. The relaxation time is the time required for a magnetization of nuclei to reach equilibrium along the magnetic field. From the relaxation times the pore volume distribution can be calculated[62].

$$\frac{1}{t} = \alpha + \frac{\beta}{r} \tag{3.2}$$

Where, t is relaxation time, r is pore size, and α and β are constants. It has advantages over the other pore characterization techniques in that it not only provides data over a larger range of pore sizes, but much larger membrane samples (~ 10cm) can be used. The size of the sample is only limited by the homogeneity of the magnetic field.

3.1.4 Permporometry

This is a flow-weighted pore size distribution test method based on gas transport rather than volume. It is best suited to gas separation applications because it is not sensitive to the amount of gas adsorbed. In this technique, a mixture of an inert gas and a condensable gas is flowed through membrane pores of various sizes and the flow measured. The gas mixture is pressurized to block the pores by capillary condensation. The pressure is then

decreased incrementally and the flow measured first in the large pores, then in the smaller ones. The pressure is decreased until there is no longer an increase in gas flow rate. The flow is measured at each pressure[63]. The change in flow rate between pressures is then related to the pore size by the Kelvin equation for capillary condensation:

$$\frac{2\cos\theta}{r} = -\frac{RT}{\sigma V}\ln\left(\frac{p}{p_o}\right) \tag{3.3}$$

Where, θ is contact angle between the liquid and the pore wall, V is the molar volume, r is pore radius, R is the gas constant, T is temperature in Kelvin, and σ is the kinetic diameter of the diffusant. The test is normally done for small pressure differences across the membrane (< 3cm Hg) and a low mole fraction (0.05-1) of condensable gas. The time required to do the analysis is dictated by temperature and pressure equilibrium times and is typically several hours. Various sizes and shapes[64-66] of membranes can be accommodated.

3.2 Characterization of the Structural Integrity of the Membrane

A method commonly termed the bubble point test is used to determine if there are any cracks or pinholes in the membrane. It is also found as ASTM F316[67] test procedure. This method relies on the Washburn equation:

$$d = 4S\frac{\cos\theta}{\Delta P} \tag{3.4}$$

Where, d is the pore diameter, S the surface tension of the liquid, θ the contact angle between the membrane and the liquid, and ΔP the applied pressure difference. It is seen that a pressure difference is required to displace a liquid from a pore with a gas such as air or nitrogen. The liquid medium is typically water. A schematic of a typical apparatus to do this type of measurement is given in Figure 3.1.

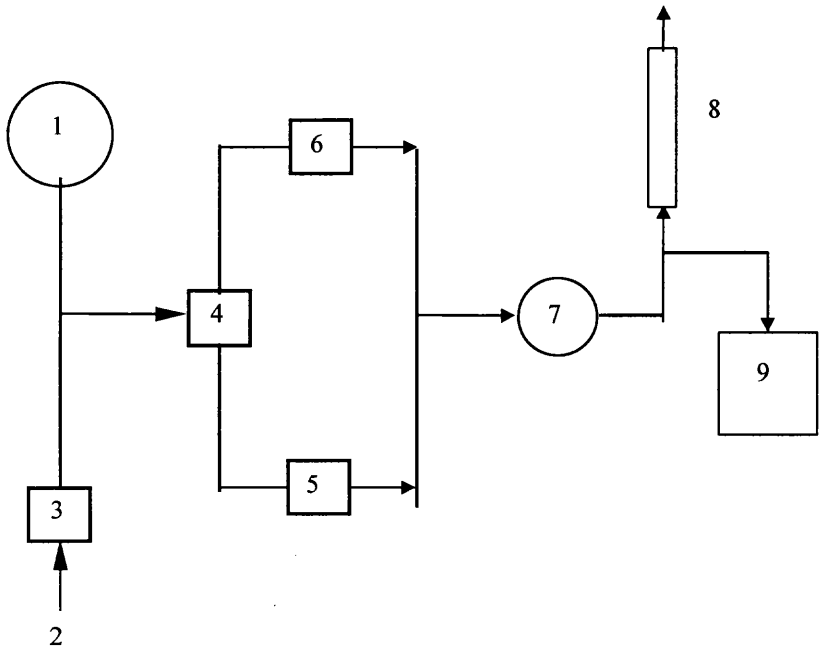

1. Pressure Gauge
2. Pressure Source
3. Pressure Regulator
4. Two-Position Valve
5. Dry Membrane Holder
6. Wet Membrane Holder
7. Liquid Trap
8. Rotameter
9. Bubble Point Detector

Figure 3.1 Schematic of bubble point test apparatus

This test is most often used to detect the largest pore size of the membrane by finding the pressure difference and thus the pore diameter at the first appearance of bubbles from the liquid-saturated membrane when the test gas pushes the liquid out of the largest size pores. If there are any cracks or pinholes in the structure, the method will notice them as the largest pores and the first bubbles will appear at a much lower pressure than usual.

3.3 Gas Separation Mechanisms and Transport Phenomena

There are many possible transport mechanisms in a gaseous system. Laminar and turbulent flows, which occur in large pores, and bulk diffusion cannot be used to separate gases. Therefore, useful transport phenomena for gas separations in porous membranes mainly rely on the following mechanisms, or some combination thereof:

- Knudsen diffusion
- surface diffusion
- capillary condensation
- size exclusion or molecular sieving

3.3.1 Gas Separation by Knudsen Diffusion

Knudsen diffusion is generally evident when the pore diameter is 5 to 10nm under pressure or 5 to 50nm in the absence of pressure. The separation factor is limited by the square root of the molecular weight ratios of the gases being separated. Therefore, it is only practical for the separation of light gases from heavy ones. Several phenomena happen in a typical gas transport[69]. Molecular diffusion is one such phenomenon that consists of molecule-molecule interactions taking place with conservation of total amount

of momentum. Next comes laminar flow or viscous flow that is due to molecule-wall interactions. In this collision, the molecule loses momentum to the wall. If there is enough interaction between rebounded and adjacent molecules, the momentum loss is progressively transferred to the bulk of the gas. Here, there is no segregation of species (as mentioned earlier) and there is a loss of momentum. Finally there is Knudsen diffusion[68]. This is again due to a molecule-wall collision, but this time there is no interaction between a rebounded and adjacent molecule. Therefore, the molecules statistically collide against the wall than with each other. There are as many gas fluxes as there are species and they are independent of one another, unlike molecular diffusion. Under pressure though, only laminar flow and Knudsen diffusion are relevant. Statistically, if the molecules collide with each other more than the wall of the membrane, the mean free path of the molecules is much smaller than the pore radius, laminar flow dominates over molecular diffusion. Only Knudsen diffusion occurs[70], if the collision of molecules with the membrane wall is greater than that with each other. The Knudsen number gives an indication of which type of flow is dominant:

$$\boldsymbol{Kn} = \frac{\lambda}{\boldsymbol{r}} \tag{3.5}$$

Where λ, the mean free path, is:

$$\lambda = \frac{\mathbf{16}\eta}{\mathbf{5}\pi \boldsymbol{P_m}} \sqrt{\frac{\pi \boldsymbol{RT}}{\mathbf{2}\boldsymbol{M}}} \tag{3.6}$$

r is the pore radius, η the gas viscosity, P_m the mean pressure, R the gas constant, T the temperature, and M the molecular mass. Knudsen diffusion occurs for Kn > 1 and is given by:

$$F_{o,Kn} = \frac{2}{3}\frac{\varepsilon \mu_k v r}{RTL} \tag{3.7}$$

Where, v is the mean molecular velocity and is given by:

$$v = \sqrt{\frac{8RT}{\pi M}} \tag{3.8}$$

$F_{o,Kn}$ is permeability, ε the porosity, μ_k a shape factor, and L the thickness of the porous medium. Gas separation by Knudsen diffusion can be determined from the ratio of permeability of two gases, A and B:

$$\frac{F_{o,A}}{F_{o,B}} = \sqrt{\frac{M_B}{M_A}} \tag{3.9}$$

Thus, separating gases according to their molecular mass.

3.3.2 Gas Separation by Surface Diffusion

Surface diffusion can be used if the gases to be separated are closer in molecular weight. Here, one component is preferentially absorbed. As it accumulates on the pore surface,

the adsorbed component diffuses faster than the other non-adsorbed component. This surface adsorption and diffusion creates a difference in permeability and therefore in separation. It generally works well when the pore diameter is 1 to 10nm or the surface area is very large[71].

Mainly, gas molecules can interact with the surface, adsorb on the surface and move along it. If a pressure gradient is present, a difference in surface occupation occurs. The surface composition gradient created allows transport to occur. The gradient in surface diffusion is known as a surface concentration gradient. The concentration of adsorbed phase is a function of pressure, temperature, and the surface itself. But, the more molecules adsorbed on the membrane, the less the likelihood they will diffuse along its surface. So, controlling the amount of gas adsorbed by the membrane is critical to optimum transport.

Another way to increase the surface diffusion is through a pore size decrease. To describe the relation between surface permeability and the structure of the porous medium for cylindrical pores, the following is used:

$$F_{o,s} \sim \frac{\mu_s \varepsilon}{r} \tag{3.10}$$

So, decreasing the pore size increases the surface area of the membrane, and surface diffusion is facilitated. Several models describing surface transport are found in the literature[15,71].

3.3.3 Gas Separation by Capillary Condensation

At low temperatures, some gases will undergo capillary condensation where they occupy the pores of a membrane as a liquid[71,72]. When other gases do not dissolve in the condensed component, separation occurs. Even though this mechanism has been widely used in separation processes involving porous adsorbents, very little is reported in the literature about the dynamic behavior of capillary condensation through porous membranes[41]. This is the pertinent application if separation is desired. However, some studies which do not correlate well with each other, exist[71].

3.3.4 Gas Separation by Molecular Sieving

Molecular sieves are porous media with pores of molecular dimensions. Selectivity is due to the size of the gas molecule. A gas with a kinetic diameter less than the pore will go through while that with a larger kinetic diameter will not. Traditionally, molecular sieves were zeolites or carbon solids[46,71]. Although much more information is needed in the way of mechanisms that affect molecular sieving, Koresh and Sofer have come up with a simplistic model describing the separation of a CH_4/H_2 mixture, Figure 3.2. It is assumed that the H_2 and CH_4 molecules reside at different minimum energy positions prior to an activated jump through a pore. The larger molecule will reside at a greater distance than the smaller molecule because of the amorphous character of the membrane.

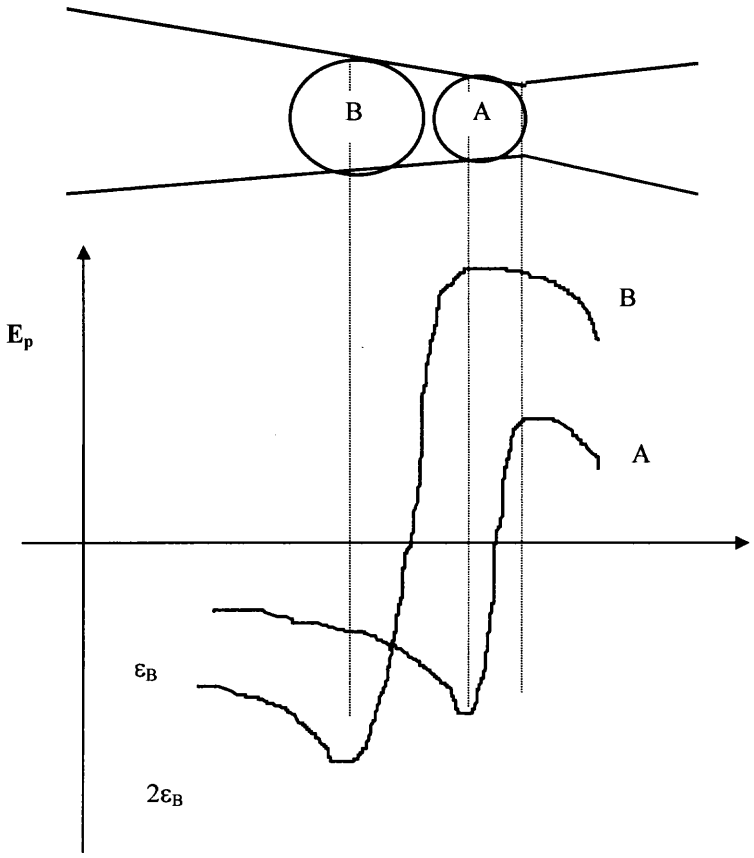

Figure 3.2 Potential energy (E_p) along the permeation path of two molecules of different sizes, representing hydrogen and methane

3.4 Entropic and Energetic Selectivity in Air Separation

As the topic of discussion is air separation, it is essential to separately discuss the role of entropic and energetic selectivity in the process[18]. The separation of gas mixtures based on differences in the diffusion rates of the constituent species through a microporous/nanoporous medium is a topic of great technological and scientific importance (Karger and Ruthven, 1992). An effective diffusivity-based separation requires a medium with pores small enough to discriminate among the different components. Separation becomes very challenging when the sizes of the species in the mixture are very similar, as in the case of oxygen and nitrogen.

A trade-off between permeability and selectivity is a limitation often encountered in the design of materials for kinetic (diffusion-based) separations; in order to increase the selectivity, the magnitude of the diffusion barrier must be increased (i.e., the pore size must be reduced). Robeson (1991) demonstrated this permeability-selectivity tradeoff. Singh and Koros (1996) pointed out that the upper bound on the performance of polymeric membranes falls short of the economically attractive region presently occupied by inorganic membranes. Furthermore, these authors analyzed experimental data within the framework of transition state theory to obtain the individual energetic and entropic contribution to the selectivity in the oxygen/nitrogen separation. Singh and Koros observed that the energetic selectivities in the inorganic sieves and polymers were of comparable magnitude, but that the performance of the inorganic materials was far superior in terms of entropic selectivities. The authors surmised that this result was due to inherent differences in the molecular-level rigidity of the host materials; the inorganic materials could effectively limit the rotation of the nitrogen molecule in the transition

state, while the polymer could not, due to the larger thermal fluctuations in the polymer matrix.

Diffusion coefficients are usually interpreted in the context of an activated process, where the diffusivity for species, i, can be expressed as:

$$D_i = D_{o,i} \exp(-U_{a,i} / k_B T) \tag{3.11}$$

Where, $D_{o,i}$ is frequency factor, $U_{a,i}$ is the activation energy, k_B is the Boltzmann constant and T is the temperature.

Following Glasstone et al. (1941), transition state theory (TST) may be used to express the frequency factor in terms of an entropic barrier $S_{a,i}$:

$$D_{o,i} = e\delta_i^{\,2} (k_B T/h) \exp(S_{a,i} / k_B) \tag{3.12}$$

Where, δ_i is the jump length and h is the Plank constant.

The entropic term can be thought of as quantifying the difference in the degree of confinement of the molecule between the transition state and the minimum. In many cases (such as oxygen and nitrogen), the jump length δ_i will be equal to a good approximation.

The diffusivity selectivity for two species A and B can then be expressed as:

$$D_A / D_B = \exp\{(S_{a,A} - S_{a,B})/k_B\} \exp\{-(U_{a,A} - U_{a,B})/k_B T\} \tag{3.13}$$

By measuring the diffusivities of both gases at several temperatures, one can calculate both the entropic and energetic contributions to selectivity through a regression analysis.

Diffusivity selectivity from transition state theory and statistical mechanics for oxygen and nitrogen is:

$$D_{O2} / D_{N2} = (m_{O2} / m_{N2})^{-1/2} Z_{A,O2} / Z_{A,N2} \qquad (3.14)$$

Where, m is the mass of molecule and Z_A is the configuration partition function for a molecule confined to window. Configurational partition functions completely account for the molecular-level energetic interactions between the gas molecule and the solid.

This detailed discussion on this advanced subject accounts to the air separation results obtained later. This selectivity characteristic could be playing a major role, other than various complex mechanisms, to arrive at the selectivities observed between oxygen and nitrogen.

CHAPTER 4

EXPERIMENTAL PROCEDURE

4.1 Modified LPCVD Reactor

The membranes in this study were synthesized in a modified LPCVD reactor as shown in Figure 4.1.

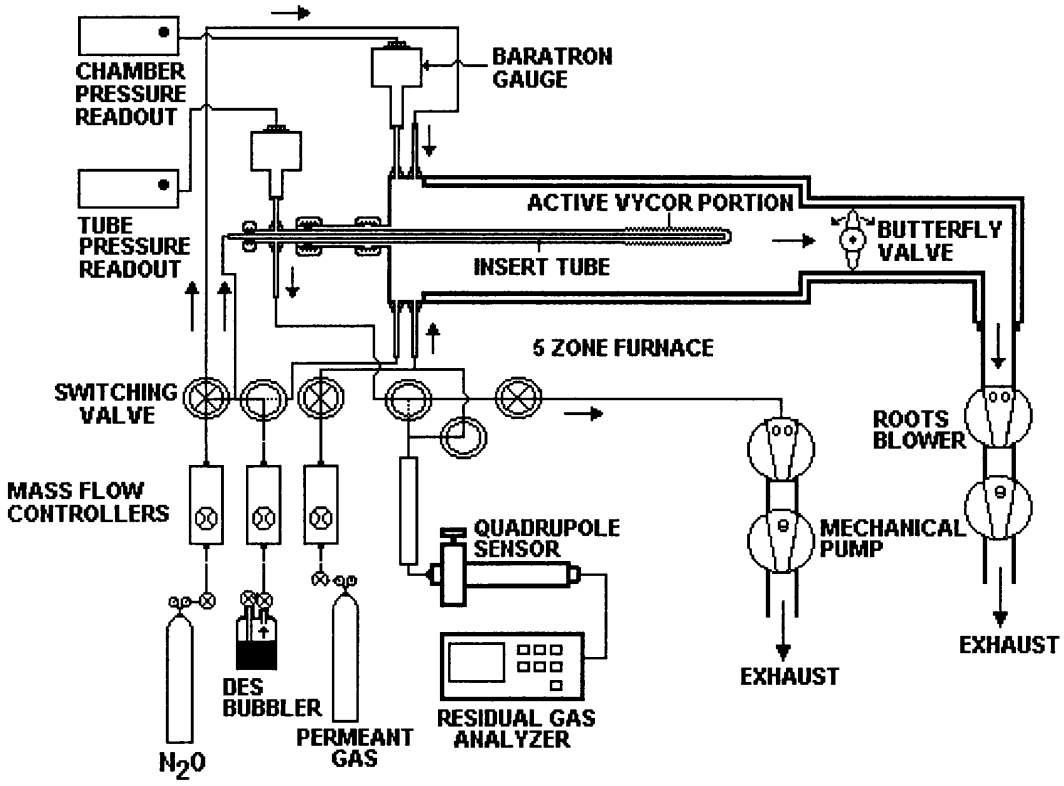

Figure 4.1 LPCVD reactor for the synthesis of SiO_2 films on Vycor tubes

The reactor was a horizontal fused quartz silica tube having an inner diameter of 19.3cm and a length of 155cm. The tube was heated in a five-zone Lindberg furnace providing a uniform temperature distribution across the reactor, heat transfer occurring by convection. This temperature distribution was measured with an Omega-type K thermocouple. In this study, only the middle three heating zones of the furnace were used. The two heating zones at the ends were kept closed and high-speed fans turned on to keep them cool and thus protect the delicate Viton O-ring gaskets sealing the quartz tube. The back end of the reactor was connected to an Edwards' vacuum system that consisted of a mechanical pump, Model E2M80, and a Roots blower, Model EH500. The other end of the reactor had a door for access to the quartz tube as well as a fixture for inserting the Vycor tube. The pressure in the reactor was monitored using a standard MKS baratron gauge and the exhaust controlled by the use of a MKS exhaust valve. Also, the reactor had an effective temperature control range up to 1200°C. However, the maximum temperature reached in this study was 550°C. This care was taken to prevent any undesirable sintering of the porous Vycor tube into a non-porous tube.

The precursor gases were DES and N_2O. DES was delivered from a temperature controlled liquid source bottle. Due to the high vapor pressure of DES a carrier gas was not required. Nitrous oxide was delivered using a high-pressure gas cylinder. The precursor gases as well as the permeant gases, were monitored using calibrated automatic mass flow controllers, Applied Materials model AFC 550. Stainless steel delivery lines were used to bring reactants and the permeate gases into the reactor.

The Mass Spectrometer, Inficon Quadrex 200, was connected to the system using a quadrupole sensor for monitoring the residual gases.

4.2 SiO_2/Vycor Membrane Fabrication

4.2.1 Predeposition Procedure

The support structure for the membranes was a porous borosilicate glass tube known as Corning Vycor Glass #7930 with a composition of 96% SiO_2 and 3% B_2O_3. The Vycor glass had an average pore diameter of 40 Angstrom and 28% porosity. The tube had an outside diameter of 0.8cm and a 0.11cm wall thickness. The tubes were cut into sections and both ends of these sections slowly heated to 1200°C to flow the glass and thus close the pores. This left an active length of 17cm. One end of the active Vycor tube length was sealed while the other was attached to a similar diameter fused silica tube. This fused silica tube held the membrane in the center of the reactor and allowed for sufficient plumbing of the reactant gases and vacuum lines.

Once prepared, this Vycor tube support structure was inserted into the system through the fixture attached to the front end of the reactor. The LPCVD chamber was evacuated and the temperature slowly raised and kept periodically constant for 15 minutes after 50°C increments until the desired deposition temperature of 550°C was reached. The entire system was pumped down overnight to ensure that all moisture adsorbed by the Vycor tube was eliminated and outgassing from the chamber walls was minimal. After the chamber and Vycor tube were sufficiently evacuated, the outgassing rate was checked by closing off all valves to the chamber and observing the pressure rise in the reactor. Typical outgassing rates were on the order of ~ 4mtorr/min.

4.2.2 SiO_2 Deposition

A counterflow geometry to initiate SiO_2 deposition was used. Levy[34] et al showed that the counterflow geometry provided membranes with better stability and selectivity. The counterflow geometry gave an optimum pore narrowing rate inside the pores of the substrate and eliminated the possibility of film cracking. Here, a long, narrow stainless steel tube was inserted inside the Vycor tube, approximately 2cm from the closed end. First, DES was constantly flowed throughout the deposition from inside the tube at a flow rate of 30sccm. The vacuum was kept open in the tube to maintain a pressure of DES inside the Vycor of 4torr. After a stable flow of DES was reached, N_2O was flowed on the outer surface of the Vycor tube at 150sccm with a pumping rate sufficient to maintain 4.8torr. N_2O has been shown to give better permselectivity results over other oxidants[34] by providing an enhanced pore narrowing rate. The idea showing that SiO_2 formation within pores is a self-limiting process also facilitated the use of N_2O as a precursor gas. Here, it was believed that at the point where the pore diameter approaches the size of the N_2O molecule, no further reactions would be expected and film deposition would automatically cease. The selection of N_2O with a diameter less than that of a typical VOC but greater than that of N_2 would block the flow of the larger sized molecules while still permitting the N_2 to flow through the membrane structure. This may not be the case, however. At the end of deposition, the reactants were turned off and the system allowed to pumpdown overnight so that it was sufficiently evacuated for permeability measurements. When the Vycor tube was finally pumped down to a pressure of ~20mtorr, the membrane was ready for in-situ permeability and selectivity measurements.

4.3 Permeability and Selectivity Measurements

Permeability measurements were done in-situ on the virgin Vycor tube (before deposition) and after each successive deposition. Selectivities were calculated from the permeability data. Typically, a pressure differential was established by introducing one of the permeant gases (O_2 or N_2) at a known pressure into the volume outside the Vycor tube and monitoring the pressure increase inside the tube (which was at a very low pressure) with respect to time. Long permeation times were required to render adsorption effects insignificant. Pumping out the reactor chamber overnight to properly evacuate the system after depositions and permeability measurements was also important in keeping adsorption effects to a minimum. The rate of increase of pressure dP/dt inside the Vycor tube was then plotted against the pressure difference created across the membrane. The slope of this plot was converted to permeability coefficients (mol/cm*min*atm) for each of the permeant gases. This calculation was done based on the known dimensions of each membrane, the volume of permeate chamber, and the temperature during the measurement. Selectivities were obtained from permeability ratios. These results were confirmed by using on-line mass spectroscopy. The main drawback to this approach was that it only considers the effect of the individual gas on the membrane, whereas interactions due to gas mixtures can behave much differently.

CHAPTER 5

RESULTS AND DISCUSSION

The purpose of this study is to observe the feasibility of using nanoporous SiO_2 membranes for air separation. Selectivity values about ten times more than those observed during Knudsen behavior were obtained and reproduced.

5.1 Virgin Vycor Tube Measurements

Permeability measurements were carried out on a virgin Vycor tube prior to SiO_2 deposition. The linear dependence of permeability on the inverse square root of molecular weight for all test gases is known as the Knudsen behavior. This is illustrated in Figures 5.1 and 5.2. The expected behavior is a result of the mesoporous characteristic of the support membrane with pore diameter of approximately 4nm[6,41].

5.2 Deposition of SiO_2 at 550°C

Membranes were produced using the "counter flow" geometry of the precursor gases keeping the deposition temperature at 550°C. DES was allowed to flow through the Vycor tube while N_2O was passed on the outside of the tube i.e. within the chamber. A flow rate of 30sccm for DES and 150sccm for N_2O was maintained during all the depositions. A counter flow geometry configuration enhances SiO_2 film growth within the pores of the substrate rather than on the surface of the Vycor tube and allows the permeability of test gases to continuously decrease with deposition time and hence effectively prevent crack formation[34].

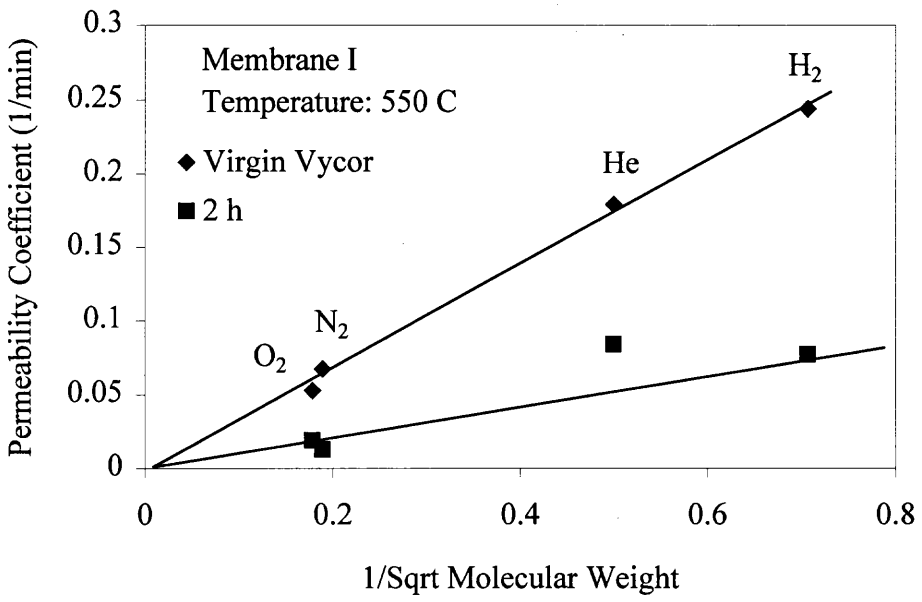

Figure 5.1 Plot of Permeability (across Membrane I) as a function of 1/Square root of Molecular weight

In order to achieve good selectivity between species of comparable size like oxygen and nitrogen it is necessary to obtain a very narrow pore size range for the membrane structure. This should be such that the final pore diameter must be larger than O_2 (kinetic diameter = 0.346nm) but smaller than that of N_2 (kinetic diameter = 0.374nm). As can be seen, the pore size range is so narrow making the situation even more challenging calling for a self-terminating situation. This is believed to occur with the use of N_2O.

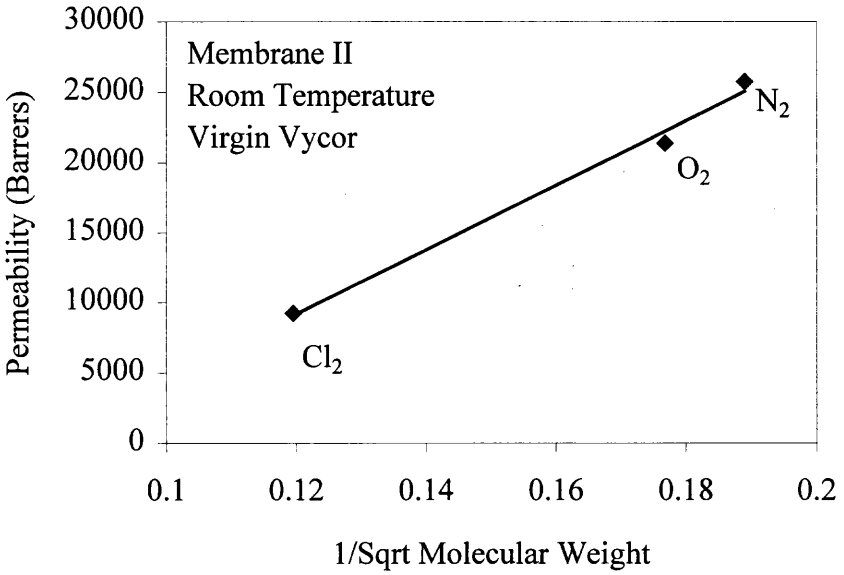

Figure 5.2 Plot of Permeability as a function of 1/Square root of Molecular weight

5.2.1 Membrane I

This membrane was produced by doing successive depositions with DES flowing inside the tube at 30sccm and N_2O outside the tube at 150sccm. DES was allowed to flow within the tube till the tube pressure stabilized at 4torr. Once this steady pressure is reached, N_2O was passed on the outside of the tube and a steady pressure of 4.4torr was observed. Deposition time was monitored when steady pressures are reached both in the chamber and tube. Successive depositions for 4 hours showed that the permeability of nitrogen was higher than that of oxygen. Both the gases showed a drop in permeability at a steady rate. After another half an hour of deposition of SiO_2 there was a steep drop in the permeability of both test gases. Oxygen and nitrogen flipped positions showing that the pore diameter has reached the point where it is smaller than that of nitrogen but is larger than oxygen. This can be seen in Figure 5.3.

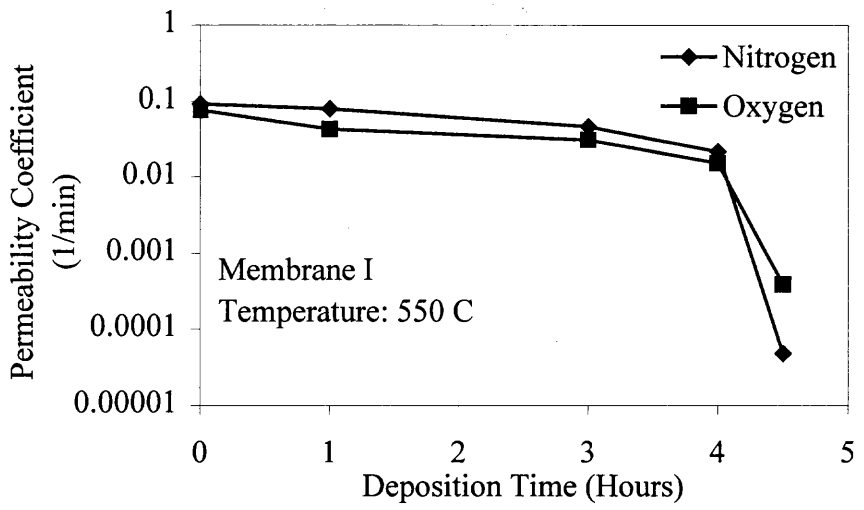

Figure 5.3 Permeability as a function of Deposition time for Membrane I

The kinetic diameter of oxygen and nitrogen are almost similar hence there is a drop in both permeabilities but the permeability of N_2 dropped by about three orders of magnitude while that of O_2 by two orders of magnitude. Figure 5.4 shows the O_2/N_2 selectivity as a function of deposition time. After 4.5 hours a selectivity of 8 was observed for $O_2 : N_2$.

As can be seen from Figure 5.5 a linear graph of dP/dt versus the pressure difference is obtained for both test gases. This shows that a very good Rsquared value~0.99 is obtained showing the accuracy of the results. All the permeability and selectivity measurements were done at 550°C.

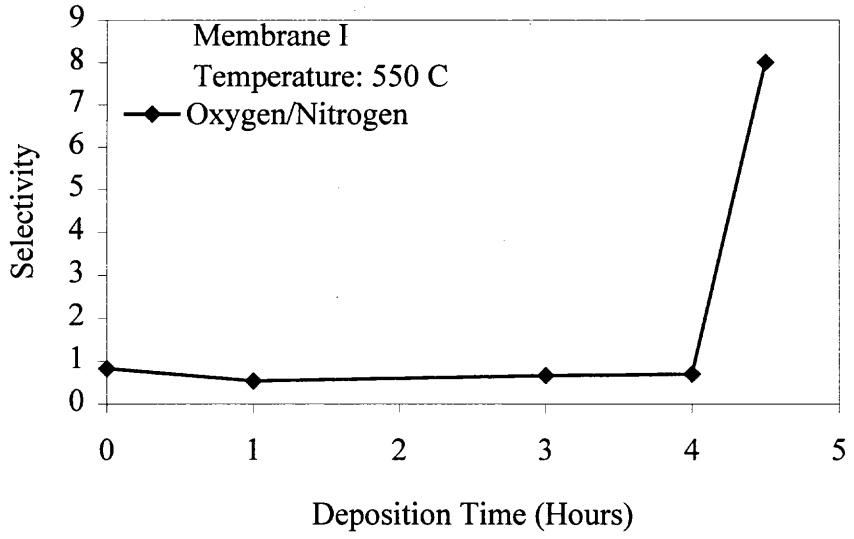

Figure 5.4 Selectivity of Membrane I as a function of Deposition time

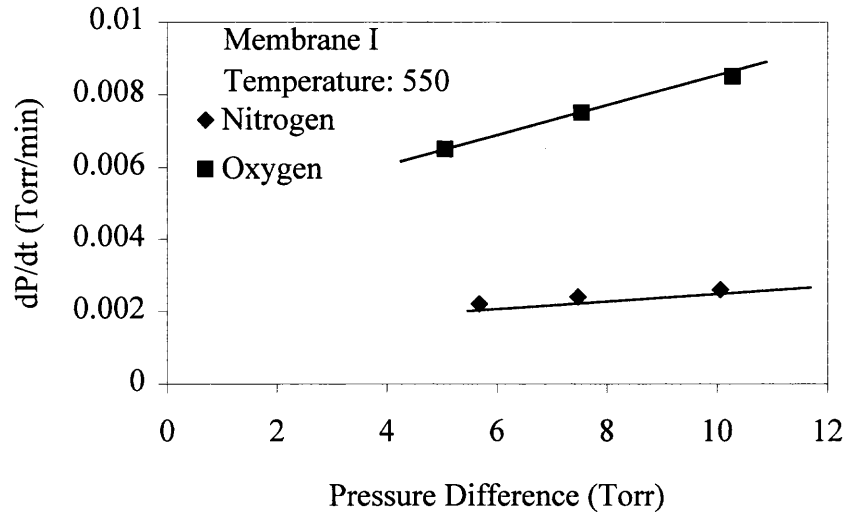

Figure 5.5 Linear dependence of dP/dt on Pressure difference for determination of Permeability for Membrane I

5.2.2 Membrane II

Deposition of SiO_2 was carried out using the same parameters discussed above. Regular depositions for shorter time intervals were carried out to precisely determine the point of best selectivity. This is illustrated in Figure 5.6 that is a plot of permeability as a function of deposition time.

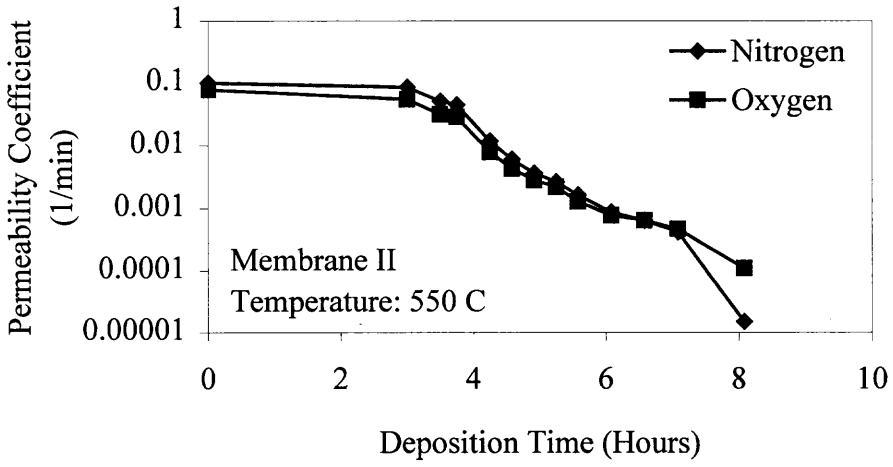

Figure 5.6 Permeability as a function of Deposition time for Membrane II

Deposition for about 8 hours was needed in this case to observe a selectivity of about 7.5 with regards to O_2 : N_2. This could be attributed to the saturation effect observed due to short deposition times. A similar flipping effect was observed and a reproducible selectivity was obtained. Figure 5.7 shows the O_2/N_2 selectivity as a function of deposition time.

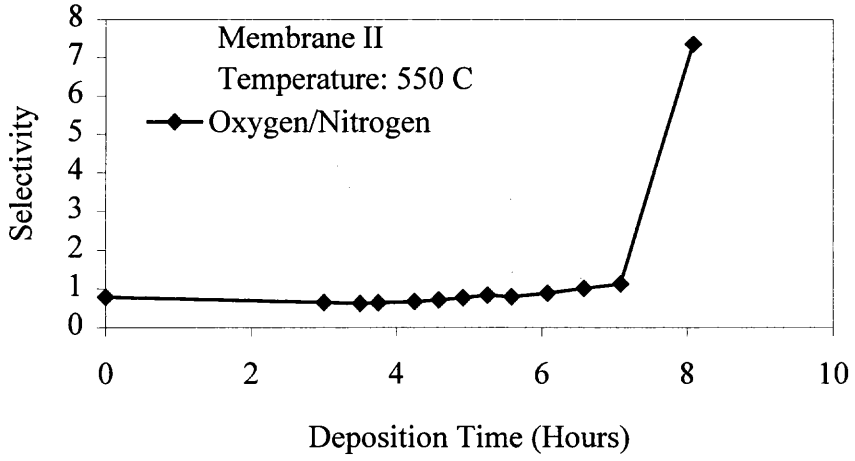

Figure 5.7 Selectivity of Membrane II as a function of Deposition time

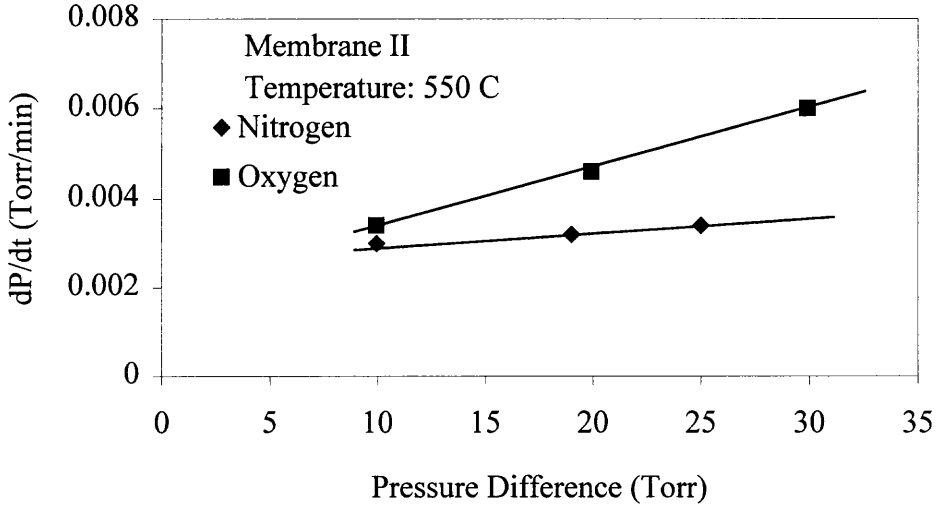

Figure 5.8 Linear dependence of dP/dt on Pressure difference for determination of Permeability for Membrane II

Again the linear dependence as shown in Figure 5.8 of dP/dt versus pressure difference shows smooth flow of the gases and a Rsquared~0.99.

To further confirm these results, an INFICON Quadrex 200 Residual Gas (quadrupole) Mass Analyzer was interfaced to the LPCVD reactor to monitor directly the composition of the gases at the feed (chamber) and permeate (Vycor tube) sides of the membrane. Mass-spec data were collected for the gas permeating through the membrane and compared with those on the inlet side. A background spectrum of the outgassing species was taken as shown in Figure 5.9. This was used to subtract from the subsequent ones. The background gas was found to be N_2 and O_2 in an 80/20 ratio, as expected.

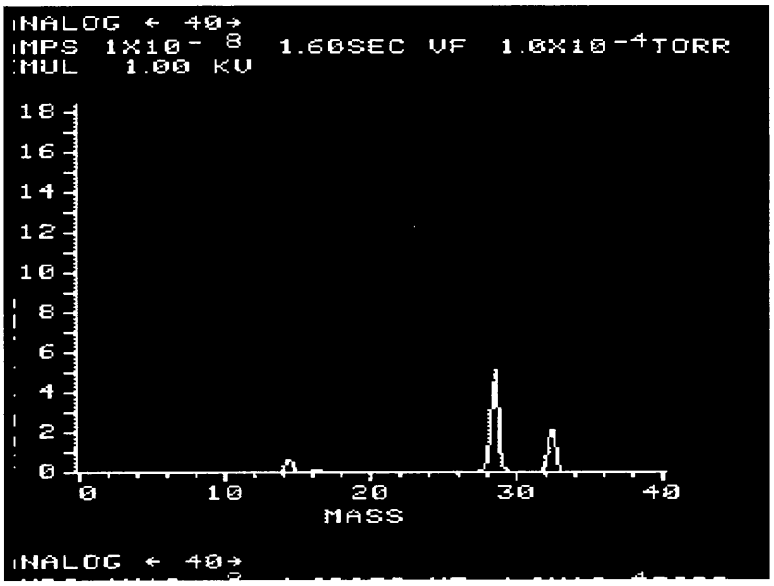

Figure 5.9 Outgassing species within the tube

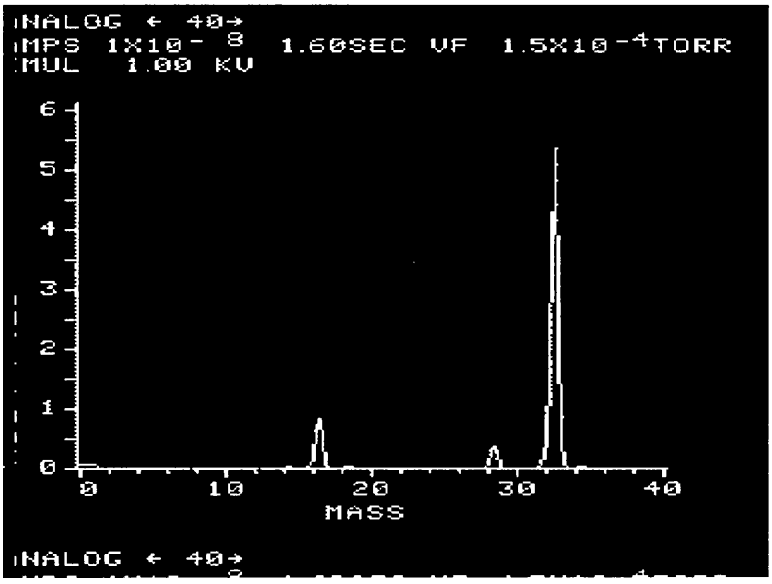

Figure 5.10 Gas sample from the tube with oxygen in the chamber

Oxygen was passed on the outside of the Vycor tube and allowed to permeate through the membrane. This gas was then tested using the mass spectrometer. The high intensity peak at a mass of 32amu showed the presence of O_2. This can be seen in Figure 5.10. When nitrogen is allowed to flow through the chamber and the gas permeating through the tube collected using the interface between the reactor and the mass spectrometer, its presence is illustrated by the peak at 28amu. The intensity of this peak is less than that of oxygen showing that a smaller amount of nitrogen permeated through the membrane. Further a higher magnification is used in this case indicating the selectivity between O_2 and N_2. Figure 5.11 illustrates the nitrogen peak.

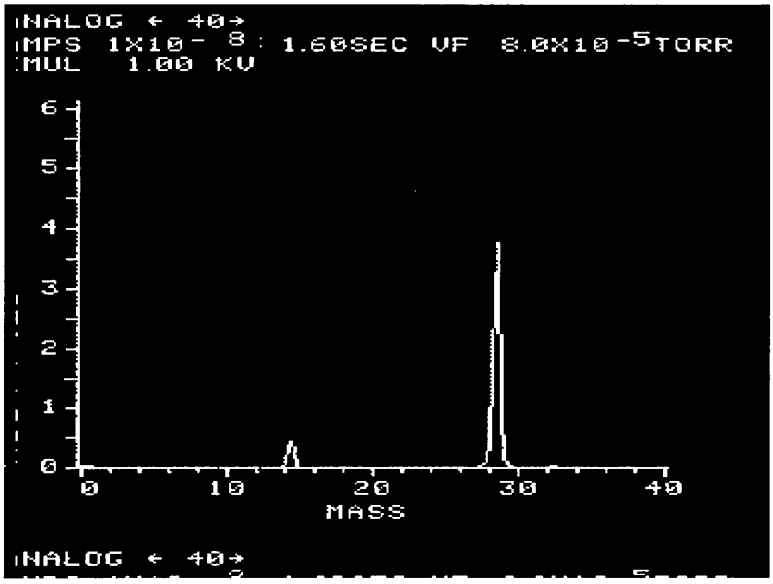

Figure 5.11 Gas sample from the tube with nitrogen in the chamber

5.2.2.1 Characterization of Membrane II: The Vycor tube was characterized using optical microscopy to observe the SiO_2 membrane. Electron microscopy imaging was tried earlier without success. Figures 5.12 and 5.13 illustrate the exterior surface or the outside of the Vycor tube. This exterior surface is observed at a magnification of 26X in Figure 5.12. To get a closer look at this surface in order to identify the coating a magnification of 54X is used in Figure 5.13. Figure 5.14 shows the interior surface of the Vycor tube. A well-defined interior coating is observed at a magnification of 54X. The cross section of the Vycor tube is seen in Figure 5.15 and Figure 5.16 at a magnification of 54X. The deposited SiO_2 film is seen at various positions along the Vycor tube.

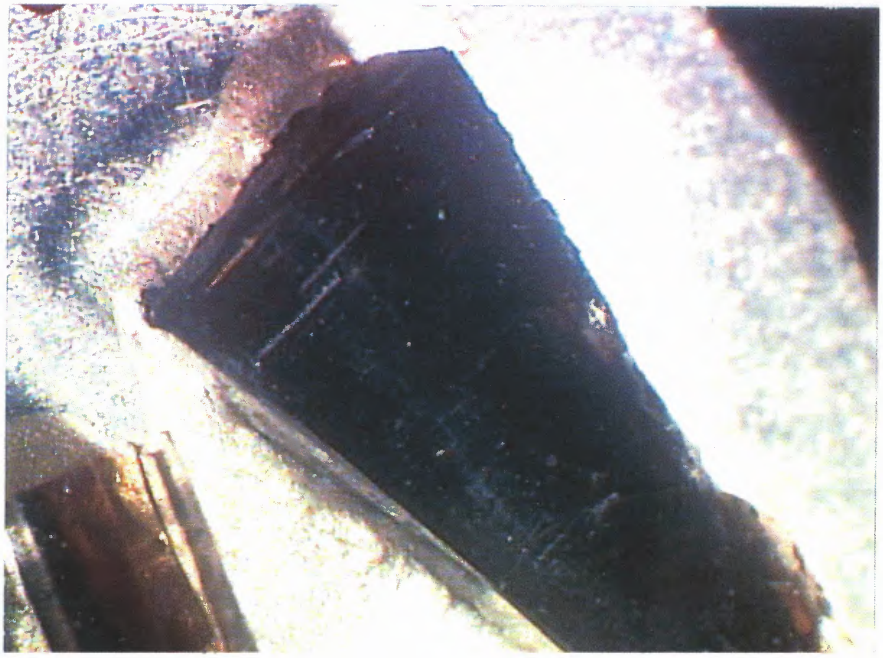

Figure 5.12 Exterior surface of Vycor tube at a Magnification of 26X

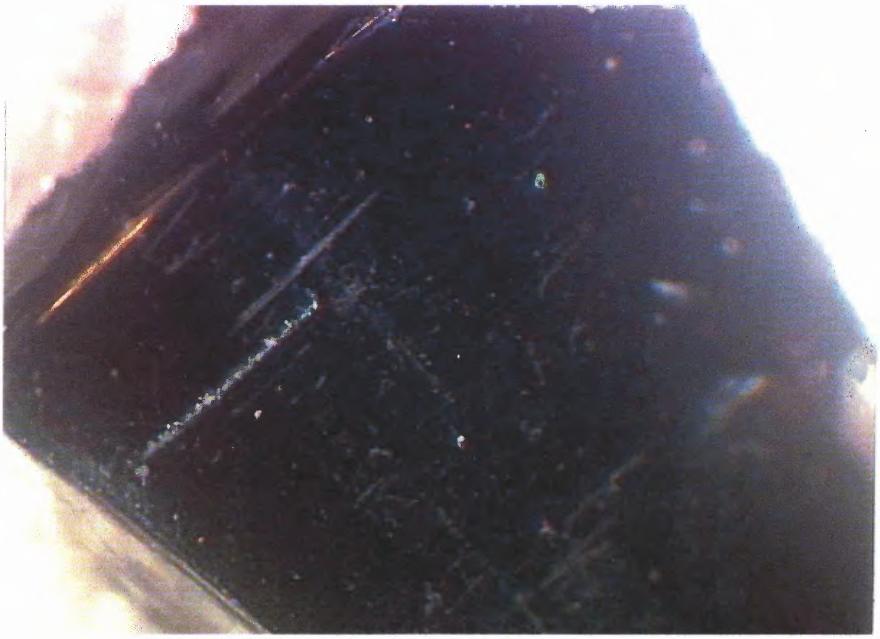

Figure 5.13 Exterior surface of Vycor tube at a Magnification of 54X

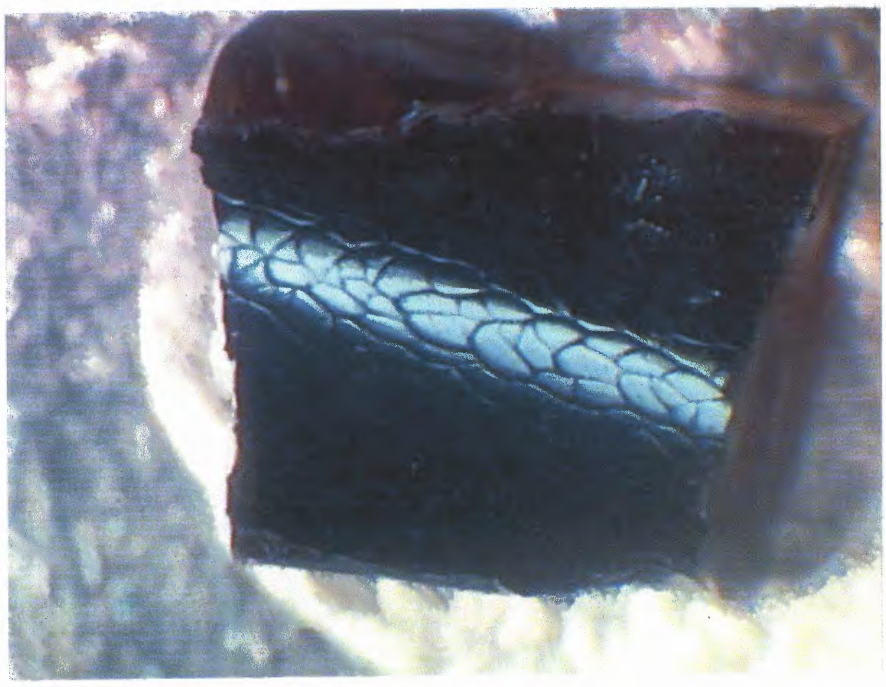

Figure 5.14 Interior surface of Vycor tube at a Magnification of 54X

Figure 5.15 Cross section of Vycor tube at a Magnification of 54X

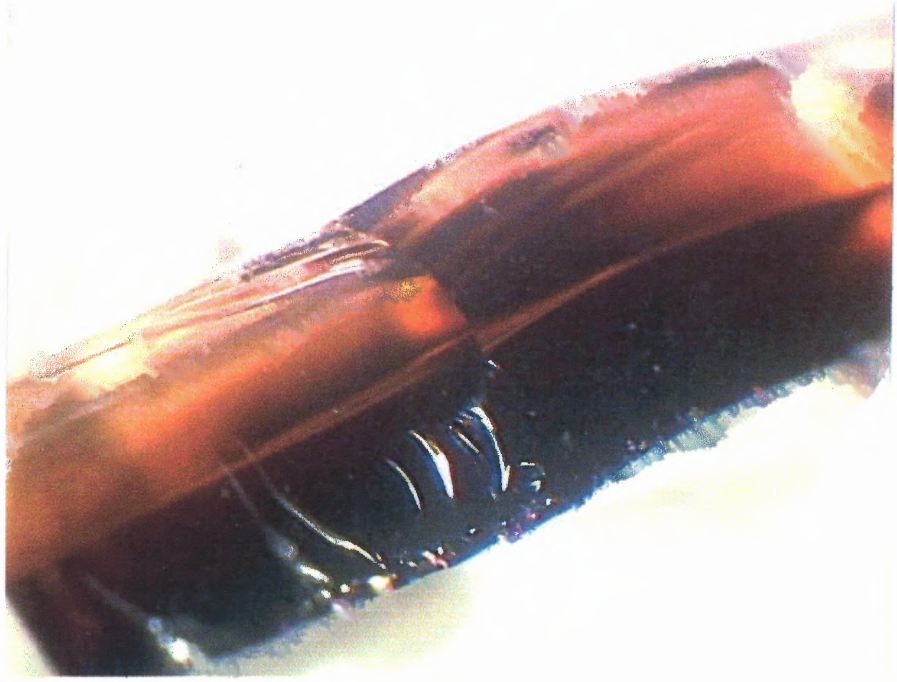

Figure 5.16 Cross section of Vycor tube at a Magnification of 54X

5.3 Effect of Temperature on Permeability

A new Vycor tube was inserted into the LPCVD reactor to determine the effect of temperature on permeability. This was done in order to see whether this temperature effect plays any role in obtaining the observed selectivity.

All fluids possess a definite resistance to change of form. This property, a sort of internal friction, is called viscosity. For gases, viscosity increases with an increase in temperature. This is illustrated in Table 5.1 for oxygen gas.

Table 5.1 Viscosity of Oxygen as a Function of Temperature

Temperature, °K	**Viscosity, g/cm-s** $10^3 \eta_0$
250	0.1780
270	0.1898
300	0.2068
320	0.2176
350	0.2334
370	0.2435
420	0.2678
450	0.2818
490	0.2997
550	0.3255
650	0.3659
750	0.4037
820	0.4290
850	0.4396

Higher the viscosity of gases, lower is their permeability through the pores of the Vycor tube. Hence, the permeability decreases with an increase in temperature. Oxygen and nitrogen were tested for permeability on a virgin Vycor tube at various temperatures. Figure 5.17 illustrates the decrease in permeability as a function of temperature.

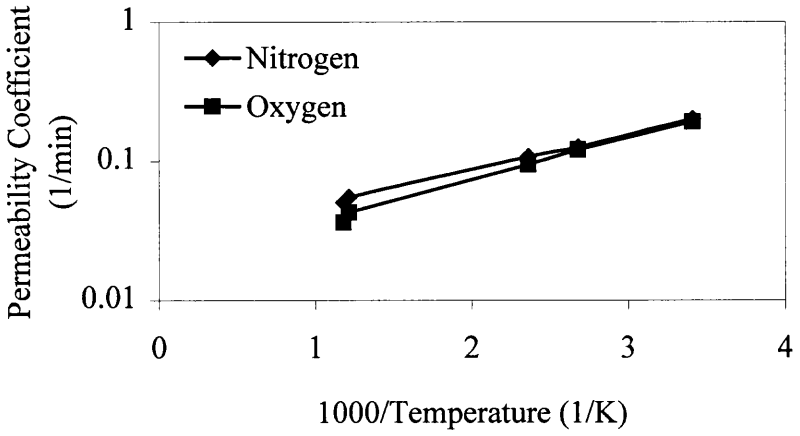

Figure 5.17 Temperature dependence of Permeability

It can be seen that the permeability of both O_2 and N_2 decreases linearly with an increase in temperature in a similar manner. Hence the observed selectivity of 7-8 between oxygen and nitrogen is independent of temperature.

5.4 Calculation of Permeability

The calculation of permeability was carried out using either of the formulae provided below. This value was converted into Barrer units.

Using ASTM standards:

$$P = \frac{\theta_p V_d T_0 l}{\Delta p A p_0 T_d} \quad (5.1)$$

θ_p = slope of downstream pressure vs. time, Torr/s

V_d = downstream volume = 40 cm^3

T_0 = STP Temperature = 273.15 °K

l = thickness = 0.11 cm

Δp = pressure differential ~ feed pressure = x Torr (x = Ave P1, cm Hg ~5, 7.5, etc)

A = surface area of membrane = 30 cm^2

p_0 = STP pressure = 1 atm = 760 Torr

T_d = Temperature of Test

P = Permeability, {1cm^3*(STP)*cm/cm^2*sec*cmHg = 10^{10} Barrers}

Referring to the article by Rao and Sircar[75], and modifying the formula using the same symbols:

$$P = \frac{\theta_p V_d T_0 l \ 1}{\Delta p A p_0 T_d V_0} \qquad (5.2)$$

θ_p = slope of downstream pressure vs. time, Torr/min.

V_d = downstream volume = 40 cm^3

T_0 = STP Temperature = 273.15 °K

l = thickness = 0.11 cm

Δp = pressure differential ~ feed pressure = x Torr (x = Ave P1, Torr ~5, 7.5, etc)

A = surface area of membrane = 30 cm^2

p_0 = STP pressure = 1 atm

T_d = Temperature of Test

V_0 = STP Volume = 22.4 litres = $22.4*10^3$ cm^3

Note the difference between the two formulae. The only difference is the inclusion of STP volume and the slope θ_p in Torr/min.

Further, $p_0*V_0 / T_0 = R = 82$ cm^3-atm-K^{-1}-mol^{-1} and P = Permeability,mol-$cm^{-1}min^{-1}atm^{-1}$

In this case, 1mol-$cm^{-1}min^{-1}atm^{-1}$ = $4.926*10^{10}$ Barrers

Both these formulae are right and the constant terms are used to observe consistency in units. The difference in the permeability values is due to θ_p. We have taken the slope of θ_p vs. Δp; the explanation for this follows.

The slope from the plot of dP2/dt vs. (P1-P2) was used in the calculation instead of simply the slope from the downstream pressure vs. time plot.

Simplifying equation (5.1),

$$\theta_p = \frac{\Delta p A p_0 T_d}{V_d T_0 l} * P \qquad (5.3)$$

P = Permeability, is essentially a constant term. Δp is not constant. By approximating it to be equal to the feed pressure would make the permeability value change.

i.e. a plot of P2 vs. time results in a slope, $m = L_p \Delta p$ where L_p constitutes the constant terms A, p_0, etc. Therefore a linear graph is not obtained.

Considering, the equation: $\theta_p = L_p \Delta p$ or $dP2/dt = L_p \Delta p$

We have 2 variables, dP2/dt and Δp giving us an equation of the type y = mx.

$$m = L_p = \frac{A p_0 T_d}{V_d T_0 l} * P \qquad (5.4)$$

Hence, a constant permeability value for a particular gas is obtained by plotting a graph of dP2/dt vs. Δp.

CHAPTER 6

CONCLUSIONS

In this study, a specific technology for synthesizing nanoporous SiO_2/Vycor membranes for air separation was devised. SiO_2 membranes were produced using DES and N_2O as precursor gases in a counter-flow geometry at 550°C. This deposition procedure provided an optimum narrowing rate of the pores eliminating the possibility of film cracking. To achieve considerable selectivity between species of comparable size like oxygen and nitrogen it was necessary for the process to be self-limiting. Hence, N_2O was used as the precursor gas.

Successive depositions reduced the pore size of the Vycor tube, thus reducing the permeability of gases. The sizes of both the test gases, O_2 (kinetic diameter = 0.346nm) and N_2 (kinetic diameter = 0.374nm), are similar and hence initially the reduction in permeability was seen to be similar. It was observed that the nitrogen permeability was always slightly above that of oxygen following Knudsen mechanism. At a certain point, when the pore size of the membrane reached that stage when the pores were smaller than N_2, the two gases flipped positions. The permeability of N_2 fell drastically compared to that of O_2 and selectivity about ten times more than Knudsen was observed. Molecular sieving along with entropic and energetic selectivities is believed to play the major role in arriving at a selectivity of 8 for O_2 : N_2. These results were reproduced and confirmed using mass spectroscopy. Characterization of the membrane using optical microscopy showed a well-defined coating of SiO_2.

The effect of temperature on the permeability of oxygen and nitrogen was analyzed. The permeability of both these gases reduced with an increase in temperature. This is due to the fact that the viscosity of gases increases with increase in temperature. As the permeability reduced linearly for O_2 and N_2, temperature does not affect the selectivity between the two test gases.

Finally a formula for determining the permeability was derived using ASTM standards and compared with the existing formula. The question revolving around the use of the slope between dP2/dt vs. (P1-P2) in the calculation of permeability instead of simply the slope between the downstream pressure vs. time plot was explained.

REFERENCES

1. C. Chiu, *Hydrocarbon Processing*, **69**, 69 (1990).

2. R. Spillman, *Chem. Eng. Prog.*, **85**, 41 (1989).

3. R. Renko, *Pollut. Eng.*, **26**, 62 (1994).

4. G. Fagliano, M. Berry, F. Bove, and T. Burke, *Public Works*, **122**, 96 (1991).

5. Y.S. Lin, W. Ji, Y. Wang, and R.J. Higgins, *Industrial and Engineering Chemistry Research*, **38**, 6, June 1999.

6. K.K. Chan and A.M. Brownstein, *Ceram. Bull.*, **70**, 703 (1991).

7. J. Fried, *Polymer Science and Technology*, Prentice-Hall, Englewood Cliffs, New Jersey (1995), ch.12.

8. R.E. Kesting, *Synthetic Polymer Membranes: A Structural Perspective*, John Wiley and Sons, New York (1985), p. 10.

9. H.P. Hsieh, P.K.T. Liu, and T.R. Dillman, *Polymer Jour.*, **23**, 407 (1991).

10. J. Schaep, C. Vandecasteele, J. Luyten, C. Dotermont, and D. Roels, *J. Membr. Sci.*, **163**, 21, November 1999.

11. *Chemical Engineering Progress*, **October 1999**.

12. K. Keizer and H Verweij, *Chemtech*, **January 1996**, 37.

13. S. Hwang and K. Kammermeyer, *Techniques of Chemistry, Vol. 7*, John Wiley and Sons, New York (1975), p.57.

14. D.W. Shaefer, *MRS Bull.*, **19**, 14 (1994).

15. R.E. Cunningham and R.J.J. Williams, *Diffusion in Gases and Porous Solids*, Plenum Press, New York (1980), p.12.

16. R.A. Ulhorn and A.J. Burggraaf, in:*Inorganic Membranes*, ed. R. Bhave, Chapman and Hall, New York (1991), p. 167.

17. A.B. Shelekhin, A.G. Dixon, and Y.H. Ma, *AIChE Jour.*, **41**, 58 (1995).

18. P.S. Rallabandi, and D.M. Ford, *AIChE Jour.*, **January 2000**.

19. S. Uemiya, *Separation and Purification methods*, **28**, 1 (1999).

20. R. Zanetti, *Chem. Eng.*, **June 9, 1996**, 19.

21. P. Maarten Biesheuvel, and H. Verweij, *J. Membr. Sci.*, **156**, 1, April 24, 1999.

22. J. Haggin, *C&EN*, **June 6, 1988**, 7.

23. J.C.S. Wu and P.K.T. Liu, *Ind. Eng. Chem. Res.*, **31**, 322 (1992).

24. A.L.Y. Tonkovich, R.B. Secker, and J.L. Cox, *Sepn. Sci. and Tech.*, **30**, 1609 (1995).

25. M.V. Volf, *Technical Glasses*, Sir Isaac Pitman and Sons (1961), p.178.

26. B. Gelernt, *Semicond. Int.*, **13**, 82 (1990).

27. A.K. Hochberg and D.L. O'Meara, *J. Electrochem. Soc.*,**136**, 1843 (1989).

28. G.S. Chakravarthy, R.A. Levy, J.M. Grow, and W.M. Attia, in: *The Physics and Chemistry of SiO_2 and the Si-SiO_2 Interface 2*, ed. C. R. Helms and B. E. Deal, Plenum Press, New York (1993), p. 165.

29. G.R. Gavalas, C.E. Megiris, and S.W. Nam, *Chem. Eng. Sci.*, **44**, 1829 (1989).

30. S.W. Nam and G.R. Gavalas, *AIChE Symp. Ser.*, **268**, 68 (1989).

31. M. Tsapatsis, S. Kim, S.W. Nam, and G.R. Gavalas, *Ind. Eng. Chem. Res.*, **30**, 2152 (1991).

32. M. Tsapatsis and G.R. Gavalas, *AIChE Jour.*, **38**, 847 (1992).

33. C.E. Megiris and J.H.E. Glezer, *Ind. Eng. Chem. Res.*, **31**, 1293 (1991).

34. R.A. Levy, E.S. Ramos, L.N. Krasnoperov, A. Datta, and J.M. Grow, *J. Mater. Res.*, **11**, 3164 (1996).

35. A.M. Gronda, S. Buechel, and E.L. Cussler, *J. Membr. Sci.*, **165**, 2, February 1, 2000.

36. A.J. Burggraaf and K. Keizer, in:*Inorganic Membranes*, ed. R. Bhave, Chapman and Hall, New York (1991), p. 21.

37. Q. Xu and M.A. Anderson, *J. Mater. Res.*, **6**, 1073 (1991).

38. E.T. Webster and C.G. Hill, *Sepn. Sci. and Tech.*, **30**, 1689 (1995).

39. M. Trocha and W.J. Koros, *J. Membr. Sci.*, **95**, 259 (1994).

40. A.J. Burggraaf and K. Keizer, in: *Inorganic Membranes*, ed. R. Bhave, Chapman and Hall, New York (1991), p. 23.

41. H.P. Hsieh, *AIChE Symp. Ser.*, **84**, 1 (1988).

42. J.J. Hammel, *J. Chem. Phys.*, **46**, 2234 (1967).

43. A.J. Burggraaf and K. Keizer, in: *Inorganic Membranes*, ed. R. Bhave, Chapman and Hall, New York (1991), p. 18.

44. V.M. Gryzanov, *Platinum Met. Rev.*, **30**, 68 (1986).

45. L.H. Lee and S.T. Hwang, *Chem. Eng. Comm.*, **44**, 121 (1986).

46. J.E. Koresh and A. Sofer, *Sepn. Sci. and Tech.*, **22**, 273 (1987).

47. M. Ohring, *The Materials Science of Thin Films*, Academic Press Ltd., London (1992), p. 79.

48. Y.S. Lin and A.J. Burggraaf, *AIChE Jour.*, **38**, 445 (1992).

49. K.F. Jensen, in: *Chemical Vapor Deposition*, eds. M.L. Hitchman and K.F. Jensen, Academic Press, Ltd., London (1993) p.31.

50. R.S. Rosler, *Solid State Tech.*, **20**, 63 (1977).

51. A.C. Adams, in: *VLSI Technology*, ed. S.M. Sze, McGraw-Hill, Princeton, New Jersey (1983), ch. 3.

52. R.C. Rossi, in: *Handbook of Thin-Film Deposition Processes and Techniques*, ed. K.K. Schnegraf, Noyes Publications, Park Ridge, New Jersey (1988), ch.3.

53. S. Middleman and A.J. Yeckel, *J. Electrochem. Soc.*, **133**, 1951 (1986).

54. C.R. Kleijn, T.H. van der Meer, and C.J. Hoogendoorn, *J. Electrochem. Soc.*, **136**, 3423 (1989).

55. A.J. Burggraff, *J. Membr. Sci.*, **155**, 1, March 31, 1999.

56. D.M. Smith, D.W. Hua, and W.L. Earl, *MRS Bull.*, **April 1994**, 24.

57. A. Bottino, G. Capannelli, and P. Petit-Bon, *Sepn. Sci. and Tech.*, **26**, 1315 (1991).

58. H.P. Hsieh, in: *Inorganic Membranes*, ed. R. Bhave, Chapman and Hall, New York (1991), p. 74.

59. J. Rocek and P. Uchytil, *J. Membr. Sci.*, **89**, 119 (1994).

60. P. Mikulasek and P. Dolecek, *Sepn. Sci. and Tech.*, **29**, 1183 (1994).
A.E. Derome, *Modern NMR Techniques for Chemistry Research*, Pergamon Press, Oxford (1987).

61. H.P. Hsieh, in: *Inorganic Membranes*, ed. R. Bhave, Chapman and Hall, New York (1991), p. 76.

62. F.P. Cuperus, D. Bargeman, and C.A. Smolders, *J. Membr. Sci.*, **71**, 57 (1992).

63. D.E. Fain, *Proc. First Intl. Conf. Inorganic Membranes*, **July 1989**, 199-205.

64. G. Cao, H.W. Brinkman, J. Meijerink, K.J. de Vries, and A.J. Burggraaf, *J. Am. Ceram. Soc.*, **76**, 2201 (1993).

65. A. Mey-Marom and M. Katz, *J. Membr. Sci.*, **27**, 119 (1986).

66. R.J.R. Ulhorn, K. Keizer, R.J. Vuren, and A.J. Burggraaf, *J. Membr. Sci.*, **39**, 285 (1988).

67. H.P. Hsieh, in: *Inorganic Membranes*, ed. R. Bhave, Chapman and Hall, New York (1991), p. 80.

68. R.J.R. Ulhorn and A.J. Burggraaf, in: *Inorganic Membranes*, ed. R. Bhave, Chapman and Hall, New York (1991), p. 156.

69. J.C.S. Wu, D.F. Flowers, and P.K.T. Liu, *J. Membr. Sci.*, **77**, 85 (1993).

70. J.D. Way and D.L. Roberts, *Sepn. Sci. and Tech.*, **27**, 29 (1992).

71. R.J.R. Ulhorn and A.J. Burggraaf, in: *Inorganic Membranes*, ed. R. Bhave, Chapman and Hall, New York (1991), ch. 6.

72. M. Asaeda and L.D. Lu, *J. Chem. Eng. Japan.*, **19**, 72 (1986).

73. C. Ravindranath, M.S. Thesis, Interdisciplinary Program in Materials Science and Engineering, New Jersey Institute of Technology, Newark, New Jersey, October 1995.

74. M.B. Rao, and S. Sircar, *Gas Sep. Purif.*, **7**, 279 (1993).

75. M.B. Rao, and S. Sircar, *J. Membr. Sci.*, **85**, 253 (1993).